Summer 8-16-2018

Experimental and Computational Studies on the Reinforcement Effect of Smooth Cord Grass (Spartina Alterniflora) on Erosion in Louisiana Coastal Marsh Creation Project

Sujan Baral

EXPERIMENTAL AND COMPUTATIONAL STUDIES ON THE REINFORCEMENT EFFECT OF SMOOTH CORD GRASS (*SPARTINA ALTERNIFLORA*) ON EROSION IN LOUISIANA COASTAL MARSH CREATION PROJECT

by

Sujan Baral, M.Sc.

A Thesis Presented in Partial Fulfillment
of the Requirements of the Degree
Master of Science

COLLEGE OF ENGINEERING AND SCIENCE
LOUISIANA TECH UNIVERSITY

August, 2018

THE GRADUATE SCHOOL

JUNE 13, 2018
Date

We hereby recommend that the thesis prepared under our supervision by **Sujan Baral**

entitled **Experimental and Computational Studies on the Reinforcement Effect of Smooth Cord Grass (*Spartina alterniflora*) on Erosion in Louisiana Coastal Marsh Creation Project**

be accepted in partial fulfillment of the requirements for the Degree of

MASTER OF SCIENCE IN ENGINEERING (CIVIL)

Supervisor of Thesis Research

Head of Department
Civil Engineering
Department

Recommendation concurred in:

Advisory Committee

Approved:

Director of Graduate Studies

Dean of the College

Approved:

Dean of the Graduate School

GS Form 13
(8/10)

ABSTRACT

Louisiana coastal saltmarshes are disappearing at an exponential rate. Even though several researches indicate that vegetation on coastal marshes protect the coast from erosion by providing soil reinforcement, wave buffering, sediment trapping and overall hydrologic regime control, the complex nature of coastal erosion process makes it too difficult to quantify the erosion resistance provided by vegetation. This research is focused on the study of soil binding ability provided by smooth cord grass, *Spartina alterniflora*, flourishing in dredged soil of Sabine Refuge Marsh Creation Project (CS-28) in Louisiana.

Field vane shear test was conducted to obtain the *in-situ* un-drained shear strength of soil vegetated by *Spartina alterniflora*. Direct shear tests on the rooted soil samples collected from the site were performed to investigate the overall effect of the roots on the shear strength of the soil.

Laboratory tensile strength tests of individual roots of different diameters were done to study the mechanical reinforcement provided by the roots. Two different root reinforcement models were used to study the correlation between the root-induced cohesion and the root tensile strength. The first model is a perpendicular root reinforcement model by Wu *et al*. (1979), which considers simultaneous mobilization of tensile strength of all roots crossing the shear plane. The second model is the Rip Root Model by Pollen and Simon (2005), which assumes progressive failure of bundled roots.

Results from the vane shear test and the direct shear test demonstrated that the roots of *Spartina alterniflora* significantly increase the shear strength of the soil. The increased shear strength for a location varied depending upon the root area ratio (RAR), depth of the soil sample, and tensile strength of the roots. The laboratory test results were compared with the outcomes from root reinforcement models to verify if the models can be effectively used to calculate net root reinforcement. Analysis using both the root reinforcement models shows overestimation of root induced cohesion and a new correlation was proposed. The discrepancies were because these models do not account for all the factors involved in the root-soil matrix.

Results obtained from a validated "Delft3D Wave-FLOW" coupled model encompassing the hydrodynamics of Lake Calcasieu estuarine system, with Hurricane Ike wave forcing condition was analyzed. Four different grid conditions were considered in the WAVE-FLOW coupled model and time-period of peak storm surge was selected to study the extreme bed stress conditions. Maximum bed shear stress and water velocity during the peak period of the hurricane was obtained at those locations from where the undisturbed soil samples were collected during the field visit. The study was done by comparing the ratio of shear strength of the soil to shear stress developed for these locations. For the different grid conditions, the ratio of shear strength to shear stress was found to be relatively higher in those grids with the presence of vegetation. This trend suggests that the significant amount of wave energy is dissipated by the presence of shoots of the vegetation.

Results from experimental tests, analytical tests and numerical analysis show the importance of *Spartina alterniflora* in enhancement of the shear strength of the soil and

in reduction of the erosive power of the waves. Thus, the study justifies the use of this marsh vegetation as a vital asset in marsh creation projects.

APPROVAL FOR SCHOLARLY DISSEMINATION

The author grants to the Prescott Memorial Library of Louisiana Tech University the right to reproduce, by appropriate methods, upon request, any or all portions of this Thesis. It is understood that "proper request" consists of the agreement, on the part of the requesting party, that said reproduction is for his personal use and that subsequent reproduction will not occur without written approval of the author of this Thesis. Further, any portions of the Thesis used in books, papers, and other works must be appropriately referenced to this Thesis.

Finally, the author of this Thesis reserves the right to publish freely, in the literature, at any time, any or all portions of this Thesis.

Author _____

Date _____

DEDICATION

To my dearest parents, ***Narayan Prasad Baral*** *and* ***Saraswati Baral****,*

The reason for what I am today.

Thanks for your unconditional love, care, and support.

TABLE OF CONTENTS

ABSTRACT iii

APPROVAL FOR SCHOLARLY DISSEMINATION vi

DEDICATION vii

LIST OF FIGURES x

LIST OF TABLES xiv

ACKNOWLEDGMENTS xv

CHAPTER 1 INTRODUCTION 1

1.1 Problem Statement and Research Need 1

1.2 Objective 3

1.3 Thesis Outline 4

CHAPTER 2 LITERATURE REVIEW 5

2.1 Background 5

2.2 Causes of Land Losses 6

2.3 Soil Erosion and Ecological Engineering 8

2.4 *Spartina alterniflora* (Salt Marsh Cordgrass or Smooth Cordgrass) 9

2.5 Root Reinforcement Models 10

2.6 The Delft3D Model 15

2.7 The Erosional Behavior of Soil 17

2.8 Analytical Erosion Model (Erodibility Index Method) 19

2.8.1 Mass Strength Number (M_s) 20

2.8.2 Block Size Number (K_B) 21

2.8.3 Discontinuity Strength Number (K_D) 22
2.8.4 Relative Ground Structure Number (J_S) 22
CHAPTER 3 METHODOLOGY 23
3.1 Site Description 23
3.2 Site Visit 25
3.3 Field Tests and Soil Sampling 27
3.4 Lab Tests 30
3.4.1 Atterberg's Limit Test 30
3.4.2 Direct Shear Test 32
3.4.2.1 Consolidation Stage: 35
3.4.2.2 Shearing Stage: 36
3.4.3 Tensile Test 38
3.4.4 Below Ground Biomass Measurement 43
3.5 Delft3D 45
CHAPTER 4 RESULTS AND DISCUSSIONS 50
4.1 Vane Shear Tests 50
4.2 Tensile Strength Test of Roots 51
4.3 Direct Shear Tests 55
4.4 Calculation of c_R and Comparison with Wu *et al*. Model and FBM Model 61
4.5 Delft3D Analysis 64
CHAPTER 5 CONCLUSION AND FUTURE WORKS 69
APPENDIX ACRONYMS, ABBREVIATIONS, AND SYMBOLS 72
BIBLIOGRAPHY 73

LIST OF FIGURES

Figure 2.1: Projected land change in coastal Louisiana from 1932 to 2050 (source: http://coastal.louisiana.gov). 6

Figure 2.2: (left) *Spartina alterniflora* growing in inner marsh; (right) *Spartina alterniflora* growing in clumps at the outer edge of the marsh..... 9

Figure 2.3: Mohr's failure envelope showing the failure envelope line with the failure zone represented by the shaded portion..... 11

Figure 2.4: A flow-chart showing the method to use the Fiber Bundle model to estimate root reinforcement coefficient (source: Pollen & Simon 2005). 13

Figure 2.5: (left) Delft3D study area shown in Google Earth enclosed by the outer black rectangle and the CS-28 Project enclosed by the inner white rectangle, (right) the WAVE Grid and the FLOW Grid (source: Shahriar 2017). 16

Figure 2.6: (a) Entrainment erosion of mud layer (b) Floc erosion (c) Surface erosion (drained failure) (d) Mass erosion (undrained failure) (source: Winterwerp & Van Kesteren 2004) 18

Figure 2.7: Graph of stream power vs erodibility Index showing the erosion threshold line represented by inclined dotted lines (source: Annandale 2006). 20

Figure 3.1: Sabine Marsh creation project (CS-28 project) in Google Maps (denoted by the rectangle in the figure), Sabine National Refuge Wildlife (denoted by the circle in the figure) and the Gulf of Mexico. 24

Figure 3.2: Enlarged view of the CS-28 project showing its five different Cycles, soil core sampling stations, and airboat route taken during soil sampling. 25

Figure 3.3 Latitudes and longitudes of soil testing and sampling points at Cycle 1..... 26

Figure 3.4: Latitudes and longitudes of soil testing and sampling points at Cycle 3. 26

Figure 3.5: (left) Vane shear testing equipment box with a torque wrench and three different sized vanes; (right) Vane shear test machine being used in the field..... 27

Figure 3.6: Bjerrum's (1972) recommended curve to calculate the correction factor for calculated undrained shear strength by Vane Shear Test. 29

Figure 3.7: (left) Using extruding rod with hammer to get soil samples from Shelby tube from inside the quadrant as seen in picture; (mid) Trimming soil samples at different depths obtained from PVC core sampler; (right) Penetrometer test being conducted on the site. 30

Figure 3.8: (left) Equipment required to conduct the liquid limit test including the Casagrande's apparatus; (right) Groove cut at center of brass cup using a grooving tool. 31

Figure 3.9: (left) Soil rolled till they crumbled in threads of size 1/8" on glass plate; (top right) Weight measurement of crumbled soil masses with the precision of three decimal places; (bottom right) Oven drying the cans to obtain moisture content. 31

Figure 3.10: The ELE international Direct Shear Machine. 33

Figure 3.11: (a) Undisturbed soil samples being extruded from Shelby tubes, (b) Rooted soil samples cut according to depths, (c) Rooted soil sample trimmed by cutter, (d) trimmed soil samples pushed inside the shear box, (e) Shear box transferred to Direct Shear Machine, (f) Direct Shear Machine during shearing phase, (g) Failed soil sample after the test showing distinct failure planes. 34

Figure 3.12: A typical consolidation curve obtained from DS-7 software during the consolidation stage of direct shear test. 36

Figure 3.13: A typical shear vs. displacement curve obtained from DS-7 software during the shearing stage of direct shear test. 37

Figure 3.14: Three different root types of *Spartina alterniflora* showing their ends being prepared for the tensile test. 39

Figure 3.15: (left) Hook arrangement for tensile test showing hooks, root samples and parts consisting of hot glue to hold the root sample; (right) Pneumatic grip arrangement showing upper and lower grips and root sample. 40

Figure 3.16*:* Electronic slide caliper used to measure the root diameters of *Spartina alterniflora.* 41

Figure 3.17: Tensile test set up using Hook arrangement before pouring hot glue at the ends of double round eye swivel (wrapped by blue tape at the bottom). 42

Figure 3.18: Failed root sample after the test showing the stretched inner vascular membranes. 42

Figure 3.19: (left) Wet washing the roots in sieve nos. #30 and #60 to separate roots from the soil; (right) Representative soil samples used to measure the underground biomass (two samples for each layer). 43

Figure 3.20: Air-drying the root samples (two from each soil layer) collected from wet sieving. 44

Figure 3.21: (left) Soil cores of each layer with roots of *Spartina alterniflora* let to air dry in the lab; (right) Broken soil core showing the roots of the plant. 45

Figure 3.22: A screenshot of Delft3D GRID showing the N value for the corresponding latitude of a sampling location. 46

Figure 3.23: A screenshot of the QUICKPLOT, showing the selected time of the peak surge and N value equal to 293 for a sampling location. 47

Figure 3.24: A graph of the maximum bed shear stress obtained from post processing tool, QUICKPLOT, for the entire range of M (longitude) and a specific value of N..... 48

Figure 3.25: A graph of magnitude of wave velocity obtained from post processing tool, QUICKPLOT, for the entire range of M (longitude) and a specific value of N..... 48

Figure 4.1: Corrected undrained shear strength profile obtained from Vane Shear Test for six different locations at the CS-28 project. 51

Figure 4.2: Graph of load vs. deformation for different root samples of root type "R_1". 53

Figure 4.3: Graph of load vs. percentage lateral deformation for different root samples of root type "R_2". 53

Figure 4.4: Graph of load vs. percentage lateral deformation for different root samples of root type "R_3". 54

Figure 4.5: Graph of root tensile strength (MPa) vs. root diameter (mm) showing the power law regression. 54

Figure 4.6: Graph of normal stress vs. shear strength for soil samples from Cycle 1 of CS-28 project. 56

Figure 4.7: Stress-Strain curve for soil samples from Cycle 1 for a normal stress of 5 kN. 56

Figure 4.8: Stress-Strain curve for soil samples from Cycle 1 for a normal stress of 11 kN. 57

Figure 4.9: Stress-Strain curve for soil samples from Cycle 1 for a normal stress of 19 kN. 57

Figure 4.10: Graph of normal stress vs. shear strength for soil samples from Cycle 3 of CS-28. 59

Figure 4.11: Stress-Strain curve, soil samples from Cycle 3 for the normal stress of 5 kN. 59

Figure 4.12: Stress-Strain curve for soil samples from Cycle 3 for the normal stress of 11 kN. 60

Figure 4.13: Stress-Strain curve for soil samples from Cycle 3 for the normal stress of 19 kN. 60

Figure 4.14: Ratio of shear strength to shear stress for six sampling locations for four different grid conditions using Delft3D analysis. 66

Figure 4.15: Graph showing the ratio of shear strength to shear stress for six sampling locations for four different grid conditions by using Annadale's Method. 68

LIST OF TABLES

Table 2.1: Mass strength number (M_s) for cohesive soil with different types of hardness (Annadale, 2006)..... 21

Table 4.1: Peak load, average root diameter, tensile strength and averaged tensile strength of roots of *Spartina alterniflora*..... 52

Table 4.2: Calculation of values of cohesion (c) and friction angle (ϕ) for different soil layers of Cycle 1..... 55

Table 4.3: Calculation of values of cohesion (c) and friction angle (ϕ) for Cycle 3..... 58

Table 4.4: Comparison of root cohesion from the direct shear test with root cohesion from Wu *et al*. (1979) perpendicular model and FBM model. 62

Table 4.5: Calculation of shear strength to shear stress ratio for six sampling locations for four different grid conditions. 65

Table 4.6: Calculation of shear strength to shear stress ratio for six sampling locations for four different grid conditions using Annadale's Method..... 67

ACKNOWLEDGMENTS

I would like to acknowledge the financial support of Louisiana Sea Grant for the duration of my MS thesis without which I would have been unable to carry out this study. I am grateful to the Costal Protection and Restoration Authority (CPRA) officials for their support and help. In an order roughly, the reverse in which I was introduced to them, I would like to thank the following people:

Mr. Mike Miller, field official at CPRA office at Lafayette, for the wonderful field trip, help and his humor.

Mr. Mark Leadon, senior coastal engineer at CPRA, for showing me the importance of coastal land in Louisiana and for showing a new world of computational modeling used in coastal engineering.

My lab mates for their advice, cooperation and help during this study.

Dr. Saurav Alam, advisor committee member, for his help and genuine interest in studying the tensile strength of the roots.

Dr. William Patterson, advisor committee member, for the huge amount of his valuable time that I took up discussing the research problems and ideas, and for providing his own backyard for numerous soil testing experiments. Thanks for showing me a different view to observe and study the soil.

Dr. Jay Wang, committee chair and advisor, for his endless patience, persistent guidance, and for believing in me. It was a great honor to have him as my advisor. My

graduate study and research would not have been successful without his vision and motivation.

Roommates, friends and faculty members at Louisiana Tech University who made Ruston feel like home away from home.

Sister, Sristi Baral and cousins, Suresh Baral and Drona Baral, for their love, support and encouragement.

And my parents, for their blessings, love and instilling in me the importance of hard work.

CHAPTER 1

INTRODUCTION

1.1 Problem Statement and Research Need

Louisiana coastal wetlands play an important role in protecting the coastal community from storm surges and flood by directly absorbing wave energy, reducing the area of open water for wind formation and by trapping sediments and acting as a natural sponge, thus maintaining shallow water depths (Costanza *et al*. 2006; Day *et al*. 2007; Moeller *et al*. 1996; Wayne 1976). It is estimated that one hectare of wetland area in Louisiana can provide net annual benefits of about $1,749 (equal to about $450K per sq. miles) because of storm surge reduction (Costanza *et al*. 2008).

Study shows that coastal Louisiana is suffering a severe land loss over the years due to erosion, subsidence, sea level rise and construction of levees on the Mississippi River. Louisiana coast is losing land at an alarming rate of 16.57 $\pm$3.26 mi^2 per year, which is analogous to losing an area the size of one football field per hour *(Couvillion et al.* 2011). This has made the coast more vulnerable to storms, submergence and further land loss. The aftermath of 2005 and 2008 hurricanes further demonstrated the importance of the coastal Louisiana in the protection of civil and energy infrastructure, shipping and fisheries industries and safety of coastal communities. However, a recent study on change in Louisiana wetlands from 1932 to 2016, by Couvillion *et al.* (2017),

which was based on historical surveys, aerial and satellite imagery, showed a decrease in rate of wetland loss. This slower rate was equivalent to losing an American field of coastal wetland in every 100 minutes (Couvillion *et al.* 2017). The study also claims that these gains are just short term and is affected by lack of major storms in the recent 8 years, recovery of land loss from 2005 hurricanes, reduction of petroleum exploration, and restoration activities (Couvillion *et al.* 2017).

In this scenario, there is a strong need to act on the protection of the coastal wetlands. Several projects are being implemented by both federal and state organizations to help reverse land loss and restore the degraded coastal ecosystem. The 2017 Coastal Master Plan formulated by Coastal Protection and Restoration Authority (CPRA 2017) encompasses projects like sediment diversion, marsh creation, shoreline protection, structural protection, barrier island/headland restoration, ridge restoration, etc. Approximately $17.1 billion out of a total of $50 billion is allocated for marsh creation projects using dredged sediments in the 2017 Coastal Master Plan. It is estimated that these marsh creation projects along with other sediment diversion projects will help to maintain or create approximately 800 square miles of land in 50 years' time (CPRA 2017).

Marsh creation project includes the dredging and transportation of sediments to the designated fill areas where the sediments are poured and let to settle and stabilize over time. The complexity and requirement to handle millions of cubic feet of sediments makes these projects one of the most expensive projects in the current master plan. These projects require long term monitoring which directly affects large coastal area and human population. This makes it difficult to monitor and quantify the impact of these projects.

As most of the marsh creation projects have been around less than 10 years, there is a lack of proper benchmark to measure the extent of success of such projects (Streever 2000).

The importance of vegetation on slope stability and erosion control has been widely studied and discussed (Coppin & Richards 1990; Gray & Sotir 1996; Greenway 1987; Waldron 1977; Wu *et al.* 1979). The strength of the created marsh depends upon the innate shear strength of dredged soil mass and the reinforcement added by the marsh vegetation flourishing on them. Recent studies of the likes of Day *et al.* (2000); Howes *et al.* (2010); Turner (2011) have shown the interdependence of soil strength and marsh vegetation.

Hence, for the sustainable and resilient constructed marsh land, the strength provided by the soil mass and vegetation should be properly understood. As such, the study of erosion resistance capability of native vegetation "*Spartina alterniflora*" on the established dredged marsh land in the Louisiana coast is deemed timely and necessary.

1.2 Objective

The overall goal of this task is to study the soil binding ability provided by *Spartina alterniflora* in dredged lands in coastal Louisiana. The research objectives can be summarized by following:

1. To perform *in-situ* tests and direct shear tests on rooted soil samples to estimate the soil reinforcement provided by roots of *Spartina alterniflora*.
2. To conduct tensile strength tests of the roots of *Spartina alterniflora*.

3. To use different root reinforcement analytical models to quantify the net soil reinforcement provided by roots of *Spartina alterniflora*.
4. To do analysis of Delft3D WAVE-FLOW coupled model with wave forcing conditions of Hurricane Ike to evaluate the erosion resistance added by vegetation on coastal soils.
5. To use the finite element analysis method to study vegetation reinforcement by considering the wave propagation along the marshland bed.

1.3 Thesis Outline

This first chapter presents the problem statement, introduction and the research objectives.

Chapter 2 mainly provides relevant literature review on general background on coastal land loss, soil shear strength, reinforcement provided by vegetation and about the analytical root reinforcement models used in this thesis. It also provides general information about Delft3D model.

Chapter 3 describes site characteristics, soil type, methods and materials used during the field visits. It presents methods and materials used to conduct vane shear test, direct shear test and tensile strength test. It also discusses the Delft3D hydrodynamic model and different wave forcing condition of hurricane Ike used in the model.

Chapter 4 presents the results and analysis obtained from vane shear test, direct shear test and tensile strength test. Furthermore, the chapter discusses the analytical analysis of the results obtained from Delft3D.

CHAPTER 2

LITERATURE REVIEW

2.1 Background

Coastal Louisiana is disappearing. The State of Louisiana that consists of forty percent of total coastal wetland within the lower forty-eight states is suffering from eighty percent of the total U.S. wetland losses (Boesch *et al*. 1994; Day *et al*., 2000).

The study done by Barras (2009) has calculated an annual loss of 29.9 sq. mi of coastal land during the years from 1978 to 2000. Recent research shows that Louisiana had lost 1883 sq. mi of its coastal wetlands from 1932 to 2010 which is equivalent to a decrease of about 25 percent of the total land area in year 1932 (Couvillion *et al*. 2011). The trend analysis shows that this loss is equal to a land loss rate of 16.57 $\pm$3.26 sq. mi per year which is analogous to losing an area of 360 ft x 160 ft (size of one football field) per hour (Couvillion *et al*. 2011).

It is predicted that the state will lose additional 513 sq. mi of wetland between the years of 2000 to 2050 (Barras *et al*. 2003). **Figure 2.1** shows the projected land change in coastal Louisiana from 1932 to 2050.

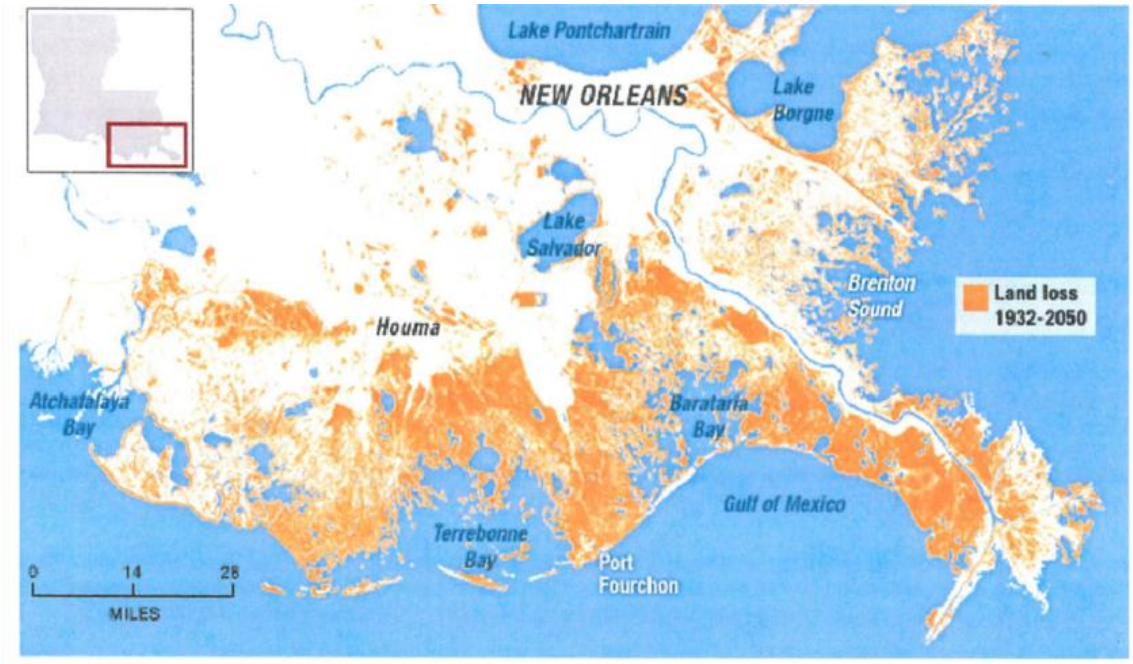

Figure 2.1: Projected land change in coastal Louisiana from 1932 to 2050 (source: http://coastal.louisiana.gov).

2.2 Causes of Land Losses

Sediments and nutrients carried by the Mississippi River are the building blocks for Louisiana wetlands. The Mississippi River replenished these wetlands with fresh water, sediments, and nutrients by either overflowing its banks or by changing its course. In response to the great flood of 1927 of the Mississippi River, flood protection system was implemented by the United States Army Corps of Engineers (USACE) that constructed levees and floodways on Mississippi River, thereby directing the river in a fixed course (Barry 1997). This had substantially decreased the amount and pattern of sediments, nutrients and freshwater reaching these deltas. In the absence of these sediments, nutrients and freshwater, these wetlands are disappearing at a staggering rate (Barry 1997; Boesch *et al*. 1994). These sediments are now discharged into the Gulf of

Mexico where the continental shelf is too deep to form the new wetlands (Boesch *et al*. 1994; Day *et al*. 2000; Mitsch *et al*. 2001).

State and federal agencies have dredged over hundreds of miles of channels through the Mississippi River Delta for navigation, drainage, logging and oil and gas development (Boesch *et al*. 1994). Other activities like land reclamation projects, coastal dredging for oil and gas exploration, rapid urbanization, etc., have severely altered wetland hydrology, changed water and sediment flow pattern and caused saltwater intrusion into the freshwater inner marshes (Houck 1983; Turner *et al*. 1984). These processes are adverse to a functional coastal ecosystem causing acres of wetlands to either change to open water or uplands (Reed & Wilson 2004).

Subsidence is the other major factor of land loss in Louisiana, which is caused by shallow processes (compaction of surface sediments, fluid withdrawal for oil and gas activity (Morton *et al*. 2002), intermediate process (compaction of sediments) and deep-seated process of tectonic origin (faulting and cyclonic down warping of crust due to regional loading) (Dixon *et al*. 2006; Shinkle & Dokka 2004). Louisiana is subsiding on average of 1.5 mm/yr., as high as 8 mm/yr. in New Orleans and as high as 25 mm/yr. in some places in the Mississippi River delta region and in Chenier plain of southwest Louisiana (Dixon *et al*. 2006; Shinkle & Dokka 2004). Subsidence is further exacerbated by rapid a sea level rise of a rate about 2-3 mm/yr. which has increased by three-fold than during the time of delta-plain formation (Kemp *et al*. 2011).

Other major factors for Louisiana coastal land loss include hurricanes, tropical storms and oil spill. Hurricanes Katrina and Rita alone eroded about 100 km^2 of land (Day et al. 2007) . Likewise, coastal Louisiana is further damaged by oil spill disasters

like the Deep Water Horizon oil spill which had spilled about 5 million barrels of oil adversely affecting Louisiana's coastal land (Crone & Tolstoy 2010; McNutt *et al*. 2012; Owens *et al*. 2011).

2.3 Soil Erosion and Ecological Engineering

Erosion of soil is defined as gradual degradation of top material from soil mass due to natural agents like wind or water. Soil erosion at the coast is believed to occur whenever the soil's ability to resist erosive failure (i.e., the resistance of a soil to shear failure) is exceeded by the energy of flowing water (i.e. the driving force exerting flow shear stress to soil surface). Ecological engineering is defined as "the design of sustainable ecosystems that integrate human society with its natural environment for the benefit of both" (Mitsch & Jørgensen 2004). Importance of vegetation on slope stability and erosion control has been widely studied and discussed (Coppin & Richards 1990; Gray & Sotir 1996; Greenway 1987; Waldron 1977; Wu *et al*. 1979). Gedan *et al.* (2011) have categorized resistance of marshes against erosion in direct and indirect mechanism.

The direct strength of below ground biomass of plants is contributed directly by plant roots which by enhancing cohesion and tensile strength of soil increases the overall shear strength of soil (Gabet 1998; Micheli & Kirchner 2002; Waldron 1977; Wu *et al*. 1979). Roots of plants can also act as a physical barrier between soil and water thus stabilizing tidal creeks (Mazda *et al*. 2007). The aboveground stem of *Spartina alterniflora* reduces water velocity, turbulence and bed shear stress and thus helps in settling and trapping of the sediments carried by flowing water (Christiansen *et al.* 2000; Redfield 1972). Indirectly, decaying plant parts by building peats increase the vertical accretion rate of the wetland (Le Hir *et al*. 2000). Decaying plants in a long term helps to

build the substrate by providing organic matter essential to the soil (Mudd *et al.* 2010; Redfield 1972). The increasing vertical accretion forms shallow water depth which has higher bed friction that reduces wave heights and attenuates the wave energy (Gedan *et al.* 2011; Le Hir *et al*. 2000).

2.4 *Spartina alterniflora* (Salt Marsh Cordgrass or Smooth Cordgrass)

Spartina alterniflora, commonly known as smooth cord grass or saltmarsh cord grass, is a dominant emergent grass species which is native to the Atlantic and Gulf coasts. Found commonly in low marsh areas of intertidal wetlands which are frequently flooded, these plants grow taller at the outer edge of marshes and shorter inwards in the marshes. It has hollow stems, flat tapered long leaves and dense rhizomatous root networks. **Figure 2.2** shows a marsh of *Spartina alterniflora* growing in the CS-28 project site.

Figure 2.2: (left) *Spartina alterniflora* growing in inner marsh; (right) *Spartina alterniflora* growing in clumps at the outer edge of the marsh.

Spartina alterniflora is a robust plant which can tolerate high salinity and can reproduce easily from seeds or from its rhizoidal roots. The plant also has aerial roots which oxygenates the plants and helps the plant to survive easily in places with high hypoxia (Anderson 1974). These qualities have made *Spartina alterniflora* an excellent choice in vegetation for use in soil stabilization and marsh restoration projects (Broome *et al.* 1988; Craft *et al*. 1999, 2003; Zedler 2000). In this research, the role of *Spartina alterniflora*, one of the dominant salt marsh grasses of Louisiana coastal marshes, in increasing the resistance of marsh against erosion is studied.

2.5 Root Reinforcement Models

Waldron (1977) used the Mohr-Coulomb equation to calculate the shear strength of soil. This root reinforcement model defines the shear strength of soil based on the cohesive and frictional resistances as shown by **Eq. 2-1**:

$$\tau' = c + \sigma_N' \tan\phi \qquad \textbf{Eq. 2-1}$$

where τ' is the effective soil shearing resistance or soil shear strength, c is the soil cohesion, σ'_N is the effective normal compressive stress on the shear plane equal to difference of the normal load (σ_N) and pore water pressure (u), and ϕ is the friction angle (in degrees) of the soil. These parameters can be represented by **Figure 2.3** showing Mohr's circle and the failure plane with corresponding stresses.

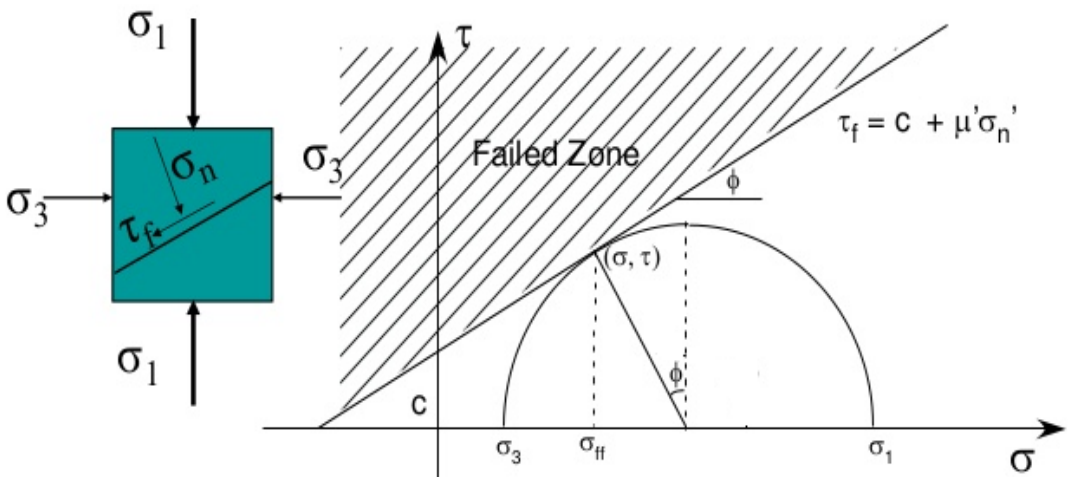

Figure 2.3: Mohr's failure envelope showing the failure envelope line with the failure zone represented by the shaded portion.

In **Figure 2.3**, τ_f is the shear strength at failure, c is the soil cohesion, $\sigma_n{}'$ is the effective normal stress and μ' is the coefficient of friction which is equal to tan ϕ. Waldron (1977) assumed root reinforcement as an additive factor to soil shear strength and extended the relation as presented by **Eq. 2-2**:

$$\tau' = c + c_R + \sigma_N' \tan\phi \qquad \textbf{Eq. 2-2}$$

where c_R is the additional shear strength increase due to presence of plant roots.

Waldron (1977) considered the roots to be cylindrical, flexible and oriented perpendicularly to the slip plane. Waldron (1977) also assumed that when the soil root matrix starts to shear, the tensile strength of all roots is mobilized. The tensile strength was then translated into the tangential component that counterbalances the shear force and the normal component which increases the confining pressure on the plane. c_R can be represented as:

$$c_R = t_R(\sin\theta + \cos\theta\tan\phi)\frac{A_r}{A} \qquad \textbf{Eq. 2-3}$$

where t_R is the tensile strength of all roots per unit area of soil, A_R/A is the root area ratio, and θ is the angle of shear distortion in the shear zone.

Wu *et al.* (1979) have shown that the term in brackets of **Eq. 2-3** ranges between 1.0 and 1.3 with normal variations in θ and ϕ (40° - 90° and 25° - 40° respectively). Wu *et al*. (1979) used a value of 1.2 to replace the bracketed term, and **Eq.2-3** was simplified as:

$$c_R = 1.2 \sum_{i=1}^{n} T_{ri}\left(\frac{A_{ri}}{A}\right) \qquad \textbf{Eq. 2-4}$$

where T_{ri} is the tensile strength of individual root (*i*), (A_{ri}/A) is the fraction of soil cross-section occupied by a single root (*i*) and *n* is the number of roots in the considered soil cross-section. **Eq. 2-4** is used in this research to quantify the root reinforcement of *Spartina alterniflora*. T_r can be correlated with the diameter of root (*d*) by power law equation as shown in **Eq. 2-5** (Gray & Sotir 1996).

$$T_r(d) = \alpha d^{-\beta} \qquad \textbf{Eq. 2-5}$$

where β and α are empirical constants varying with different plant species.

The studies done by Coppin & Richards (1990) have shown that the root reinforcement model assumes only the tensile failure of roots and it doesn't take in account the failure due to roots slipping. This results in significant overestimation of root reinforcement. Studies done by Pollen and Simon (2005) have shown that the full tensile strength of all the roots is only mobilized at a higher displacement and thus it is not fully mobilized when the soil shears. So, the assumption of failure of all the roots at the same time in Wu *et al*. (1979) model leads to overestimation of the true value of root reinforcement (Pollen and Simon 2005). To remove the limitations in Wu *et al*. model,

Pollen and Simon (2005) proposed a new root reinforcement model named the Rip Root Model. The Rip Root Model is based on the traditional Fiber Bundle Model (FBM) which assumes that the applied load is apportioned equally in all the roots in a bundle and as roots have different maximum tensile strength values, they break at different times. When the distributed load exceeds the strength of the single root strength, the root with minimum strength fails first and the load is distributed to the remaining intact roots (Pollen & Simon 2005). Failure will occur once all the roots in the bundle are broken by the acting force. **Figure 2.4** shows the steps of using the FBM method to evaluate the root reinforcement coefficient.

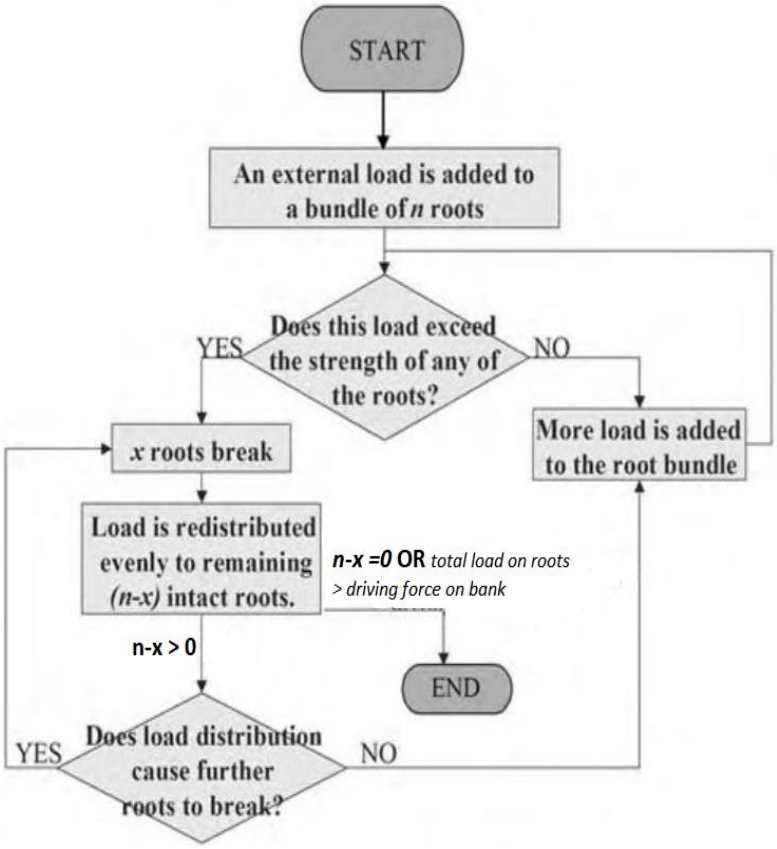

Figure 2.4: A flow-chart showing the method to use the Fiber Bundle model to estimate root reinforcement coefficient (source: Pollen & Simon 2005).

Using the limit equilibrium method, the stability of the slope can be evaluated using factor of safety (F.S.) as the ratio of the shear strength of the soil-root matrix to the acting shear forces (S_m) at the base of the slice as shown by **Eq. 2-6** and **Eq. 2-7** below:

$$F.S. = \frac{Shear\ strength\ of\ soilroot\ matrix\ (S)}{Mobilized\ Shear\ force\ (S_m)} \qquad \textbf{Eq. 2-6}$$

$$F.S. = \frac{c_R + (c + \sigma_N{}' tan\phi)}{S_m} = \frac{S_{root} + S_{soil}}{S_m} \qquad \textbf{Eq. 2-7}$$

From **Eq. 2-7**, a critical equilibrium is reached at the shear zone, when the combined shear strength of soil (S_{soil}) and shear strength contribution due to roots (S_{root}) is equal to mobilized shear force at the base of the slice (S_m).

Different methods can be used to study the soil binding ability provided by vegetation. Shahriar *et al*. (2016) evaluated the soil binding ability of Johnson grass in terms of factor of safety using the Anchor Reinforcement Method (ARM) and the Smeared Method (SM).

The ARM considered the roots as an independent reinforcing anchors between the soil layers. Cohesion (c) and friction angle (ϕ) values of plain soil sample were used for the entire soil model and the additional reinforcement provided by roots (c_R) was used as the bonding force between the soil and roots. Predetermined slip surfaces were used to calculate the factor of safety for those layers (Shahriar *et al*. 2016).

The SM considered roots as part of the soil matrix and used the overall rooted soil strength. The soil was divided into two layers with the rooted soil layer on top and the plain soil layer at the bottom. The soil layer at the top used overall cohesion (c) and friction angle (ϕ) of rooted soil and soil layer at the bottom used cohesion (c) and friction

angle (ϕ) values of the plain soil sample. Predetermined slip surfaces were again used to calculate the factor of safety for the soil layers.

Cohesion (c) and friction angles (ϕ) for both rooted and plain soil layer were obtained from direct shear tests, and numerical modeling was done using commercial software package Slope/W 2007 (Shahriar *et al*. 2016). For the pre-determined slip surfaces, comparison was made on the factor of safety for the plain soil slope and for the rooted soil slope using the SM and the ARM method, respectively. It was found that factor of safety values was much higher in case of rooted soil slope than that of plain soil slopes.

2.6 The Delft3D Model

The Delft3D is an open source modeling software package to solve the problems in sediment transport, morphology, hydrodynamics, and water quality for coastal and estuarine conditions. It consists of several open source sub-modules that can interact with each other. Among them, the hydrodynamic module “Delft3D-FLOW” allows the simulation of hydrodynamic phenomena, by solving the Reynolds-Averaged Navier-Stokes equations under the Boussinesq assumptions and shallow water assumptions. The Delft3D-WAVE module is responsible for short wave generation and propagation in nearshore areas. The WAVE and FLOW module can perform both coupled simulations (online interactions) and uncoupled simulations (offline interactions). In the coupled simulations hydrodynamic data from the Delft3D-FLOW is used by the Delft3D-WAVE module to recalculate the wave conditions.

In this study, analysis was done on the previously established Delft3D online model by Shariar (2017). The model encompassed the hydrodynamics of Lake Calcasieu

estuarine system of Louisiana. In the model, a Cartesian grid was set up along with the grid enclosure using grid generator program RGFGRID (Deltares 2011). The hydrodynamic grid of the model had nine vertical sigma layers. Bathymetry was then provided for the entire grid section. The FLOW grid covered the bathymetry of Calcasieu Lake and its flood plain. Delft3D WAVE grid was extended to an additional 8000m towards the Gulf of Mexico as shown in **Figure 2.5.**

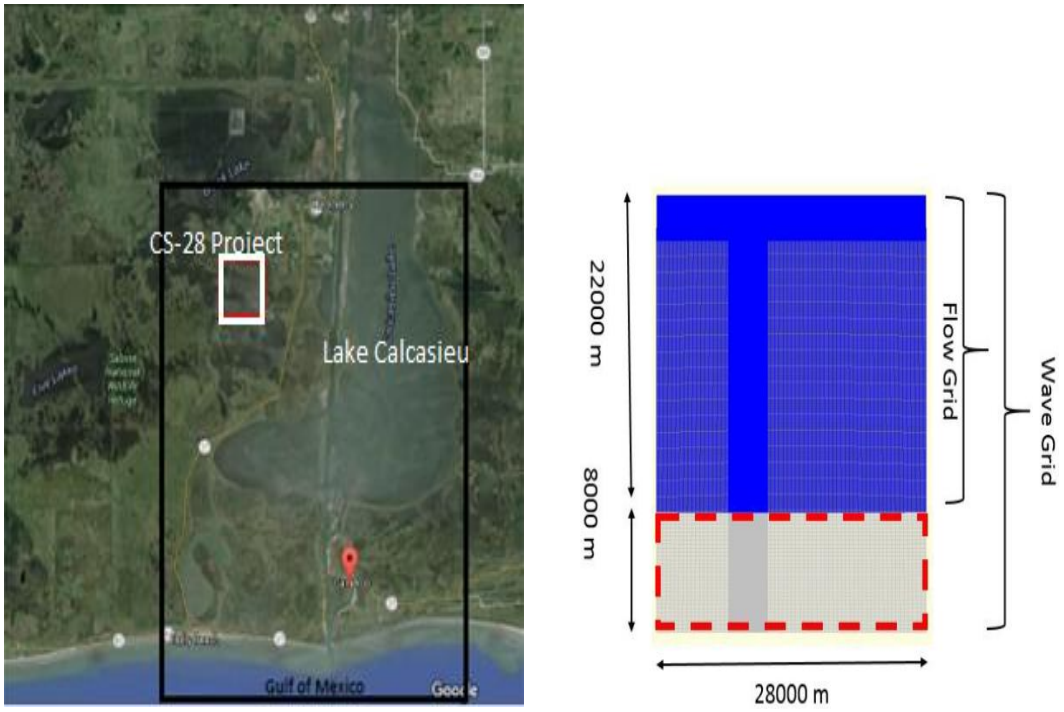

Figure 2.5: (left) Delft3D study area shown in Google Earth enclosed by the outer black rectangle and the CS-28 Project enclosed by the inner white rectangle, (right) the WAVE Grid and the FLOW Grid (source: Shahriar 2017).

To run Delft3D FLOW model coupled with WAVE model, a communication file was written and a Master Definition Wave (MDW) file was created separately, which should be executed before running the Master Definition FLOW (MDF) file. Initial

conditions include water levels, currents, water level gradients and Neumann discharge and/or Riemann boundaries. Wind and sediments processes were provided. Processes include salinity temperature, secondary flow, and constituents, etc.

The model was a coupled Delft3D-FLOW module with Delft3D-WAVE module which had the wave conditions representing that of Hurricane Ike. The model used NOAA stations and several other stations of Office of Coastal Protection and Restoration (OCPR) to obtain the tide/water level data for calibration and validation. WAVE model boundary conditions include significant wave height, mean wave period, wind velocity and directions representing the wave conditions of Hurricane Ike. The start time and stop times of the simulations were provided at the end of the model set up. In the coupled (online) process, for every communication file created, a WAVE simulation was performed. Delft3D-FLOW simulation was then resumed using the latest WAVE results.

Four different grid scenarios were studied depending upon the dry or submerged condition and vegetated or un-vegetated condition. For each sampling station, maximum bed shear stresses and velocities values during the peak surge were obtained. Results obtained were analyzed using the QUICKPLOT module, a post-processing submodule of the Delft3D.

2.7 The Erosional Behavior of Soil

Erosion process on the coast depends upon complex interaction of hydrodynamic forces, sediment bed structure and bed material properties. Erosional strength of the soil is described by Zreik *et al*. (1998) as the resistance offered by sediment bed against erosive forces. Erosion can be divided in various modes depending upon the intensity of

applied shear stress: entrainment erosion, floc erosion, surface erosion and mass erosion (Mehta 1991; Winterwerp &Van Kesteren 2004) as shown in **Figure 2.6**.

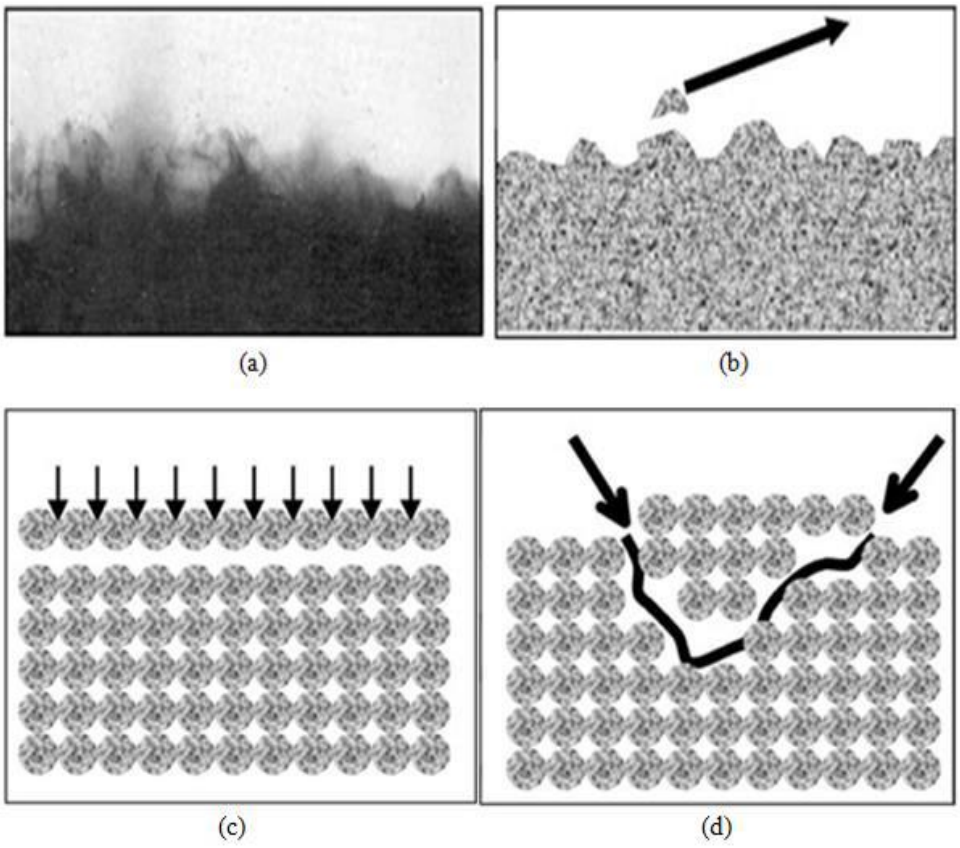

Figure 2.6: (a) Entrainment erosion of mud layer (b) Floc erosion (c) Surface erosion (drained failure) (d) Mass erosion (undrained failure) (source: Winterwerp & Van Kesteren 2004).

Entrainment erosion occurs in nature when the sediment bed is fluidized, and sediment behaves like a viscous fluid. In this type of erosion, sediment-water interface is destabilized, and fluid mud is entrained from the sediment bed. In floc erosion, bed shear stress due to fluid flow exceeds the adhesion of flocs to bed and thus removes the flocs from the sediment bed. Surface erosion is a drained failure process which occurs when

flocs attached to the sediment bed by inter-particle electro-chemical bonds break due to hydrodynamic drag and lift. On the other hand, mass erosion is the detachment of lumps of soil which occurs at considerably high shear stress greater than undrained shear strength (Millar & Quick 1998). We can take cliff erosion as an example of the mass erosion.

2.8 Analytical Erosion Model (Erodibility Index Method)

Several methods are developed to measure the erodibility of soil both analytically and numerically. These models make it easier and convenient to analyze the soil erosion resistance by accounting for soil strength. Annadale (1995) developed a semi-empirical erodibility index method to quantify the capability of soil and/or "engineered earth materials" in resisting the erosive capacity of water. Annadale (1995) gave a correlation between stream power (P) and parameter, *K*, which is defined as an erodibility index. The erosion threshold is defined by **Eq. 2-8** as:

$$P = f(K) \qquad \textbf{Eq. 2-8}$$

Critical stream power (P_c) is defined as the power of the stream at when the erosion process just starts to occur. It is the threshold power which results in the incipient motion of the soil.

For $K \leq 0.1$,

$$P_c = 0.48\, K^{0.44} \qquad \textbf{Eq. 2-9}$$

For $K > 0.1$,

$$P_c = K^{0.75} \qquad \textbf{Eq. 2-10}$$

Erodibility is the resistance of the earth material to resist erosion. Earth material will erode if $P_c > f(K)$ i.e., when the critical stream power exceeds the erodibility index

(*K*). These conditions are illustrated in **Figure 2.7** which shows the threshold line separating the scour and "no scour" conditions. Erodibility index, (*K*), is defined by Annadale (1995) as presented in **Eq. 2-11**.

$$K = M_S . K_B . K_D . J_S \qquad \textbf{Eq. 2-11}$$

where M_S is the mass strength number, K_B is the block size number, K_D is the discontinuity bond strength number, and J_S is the relative ground structure number. The description for these numbers are provided in the later pages.

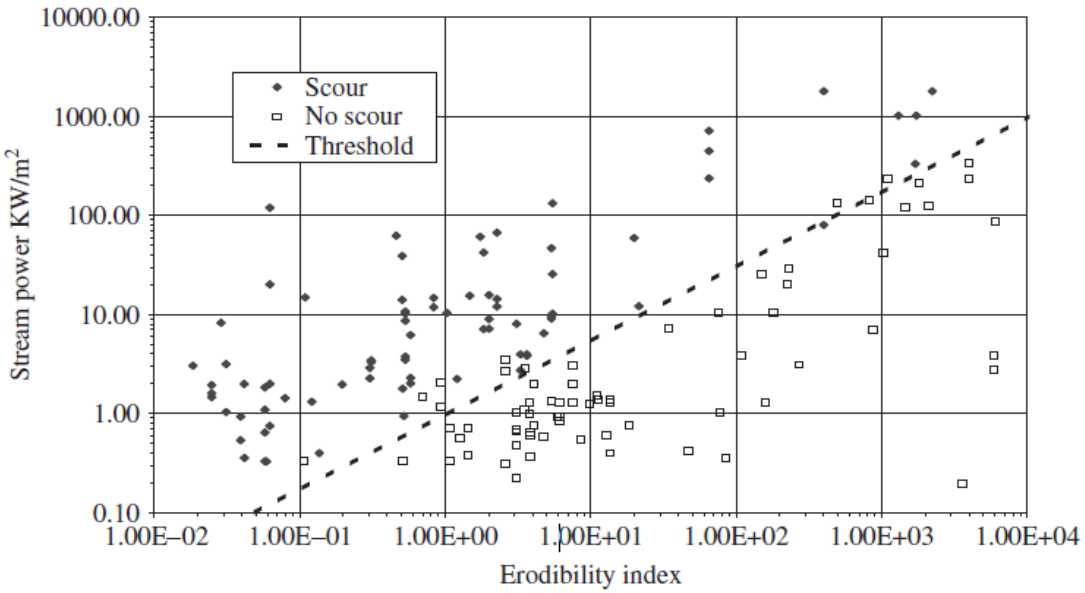

Figure 2.7: Graph of Stream Power vs Erodibility Index showing the erosion threshold line represented by inclined dotted lines (source: Annandale 2006).

2.8.1 Mass Strength Number (M_s)

Mass strength number accounts for the strength of the soil block. Annandale (2006) has given the mass strength number (M_s) for cohesive soil with different types of

hardness as presented in **Table 2.1**. Value of M_s for the cohesive soil is related to vane shear strength of the soil.

Table 2.1: Mass strength number (M_s) for cohesive soil with different types of hardness (Annadale, 2006).

Consistency	Identification in profile	Vane shear strength (kPa)	Mass strength number (M_s)
Very soft	Pick head can easily be pushed in up to the shaft of handle. Easily molded by fingers.	0–80	0.02
Soft	Easily penetrated by thumb; sharp end of pick can be pushed in 30–40 mm; molded by fingers with some pressure.	80–140	0.04
Firm	Indented by thumb with effort; sharp end of pick can be pushed in up to 10 mm; very difficult to mold with fingers. Can just be penetrated with an ordinary hand spade.	140–210	0.09
Stiff	Penetrated by thumbnail; slight indentation produced by pushing pick point into soil; cannot be molded by fingers. Requires hand pick for excavation.	210–350	0.19
Very stiff	Indented by thumbnail with difficulty; slight indentation produced by blow of pick point. Requires power tools for excavation.	350–750	0.41

2.8.2 Block Size Number (K_B)

Block size number accounts for the particle size of the soil or rock specimen. For a rock specimen, it is the function of the rock joint spacing and the number of joints. For cohesionless soil, it is a function of the size of the particle and for cohesive soils, it is assumed to be equal to one.

2.8.3 Discontinuity Strength Number (K_D)

It accounts for the relative resistance offered by the discontinuities in rock. In case of granular earth materials, it accounts for the interparticle bond shear strength. For cohesive soils, discontinuity strength number is calculated as given by **Eq. 2-12**:

$$K_D = tan\ \phi \qquad \textbf{Eq. 2-12}$$

where ϕ is the friction angle of the soil.

2.8.4 Relative Ground Structure Number (J_S)

This parameter is the function of dip value and dip direction of the least favorable discontinuity respect to the direction of the flow and the shape of the material. When using this parameter for intact materials like massive rock or clay, the value of J_S is taken equal to 1.0. With the above equations and values, erodibility index value for a cohesive soil can be obtained by using **Eq. 2-11**.

In this research, result analysis of coupled Delft3D-FLOW module with Delft3D-WAVE module was done. The WAVE module had the wave conditions representing that of Hurricane Ike. The coupled model encompassed the hydrodynamics of Lake Calcasieu estuarine system. Maximum bed shear stress and velocity of the waves on the soil bed developed during Hurricane Ike were obtained for specific locations. The erodibility index of the soil at the coast is calculated using the values given by Annadale (1995) for the cohesive soils.

CHAPTER 3

METHODOLOGY

This chapter gives the outlines of the methods employed to do various *in-situ* tests, lab tests, and fine element analysis. The chapter starts with site description which is followed by the procedures for field tests and sampling. Method for different laboratory tests is provided next, which includes soil characterization, direct shear tests of undisturbed soil samples and tensile strength tests of root samples. The last part of this section provides the description of methods used to analyze the results from a validated Delft3D model.

3.1 Site Description

Sabine Refuge Marsh creation project (CS-28) is located at the north-east of the Sabine National Wildlife Refuge, south of Black Lake and west of LA Highway 27 in Cameron Parish, Louisiana. This parish, which lies at the southwest is the largest parish in Louisiana by land area. The project involves the design of five different Cycles for the whole marsh creation project of which Cycle 1 and Cycle 3 were selected in this study.

Construction of Cycle 1 was completed on February 2002 which created 214 acres of marsh by dredging sediments from Calcasieu River Ship Channel into the shallow open water area within the retention dikes (Miller 2014). Cycle 3 was completed on March 2007 by again dredging sediments from Calcasieu River Ship Channel creating 232 acres of marsh (Miller 2014). For both projects, *Spartina alterniflora* was planted

along the perimeters. The project objective was to block saltwater intrusion inside the marshes, to construct new marsh ecosystem and to protect the marshes from erosion. **Figure 3.1** shows the Sabine Marsh creation project (CS-28) in Google Maps (denoted by the red rectangle), Sabine National Refuge Wildlife (denoted by red circle) and Gulf of Mexico.

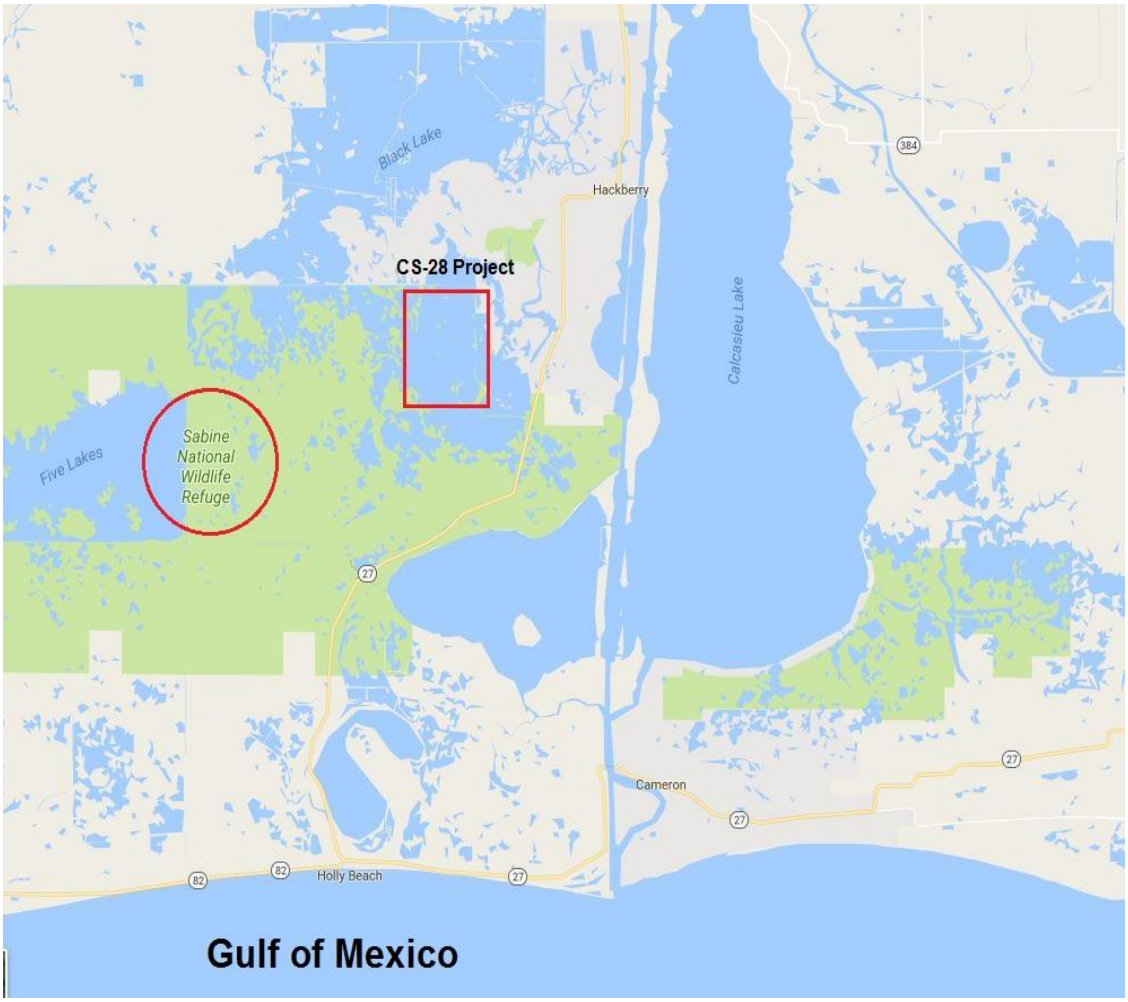

Figure 3.1: Sabine Marsh creation project (CS-28 project) in Google Maps (denoted by the rectangle in the figure), Sabine National Refuge Wildlife (denoted by the circle in the figure) and the Gulf of Mexico.

3.2 Site Visit

Site visit was done in March 2017, which was supervised by Mr. Mike Miller from CPRA Lafayette field office. An airboat was used to reach different testing locations in the marsh with *in-situ* test equipment and sampling equipment. Study site (CS-28) and its enlarged view showing the airboat route is presented in **Figure 3.2**. Three sampling locations were selected in Cycle 1 and Cycle 3, respectively. For each of the locations, *in-situ* soil test was done and followed by obtaining undisturbed soil samples using PVC cores. Locations were so determined so that they could well represent the overall project area. **Figure 3.3** and **Figure 3.4** show the latitudes and longitudes of all the sampling locations in Cycle 1 and Cycle 3 of the CS-28 project, respectively.

Figure 3.2: Enlarged view of the CS-28 project showing its five different Cycles, soil core sampling stations, and airboat route taken during soil sampling.

Figure 3.3 Latitudes and longitudes of soil testing and sampling points at Cycle 1.

Figure 3.4: Latitudes and longitudes of soil testing and sampling points at Cycle 3.

3.3 Field Tests and Soil Sampling

For each of the testing site, the vane shear test was done to measure the undrained shear strength of the soil. Undrained shear strength is the strength of the soil when rapid loading condition is applied to saturated soil in such a way that there is less time for the soil to drain. Vane Tester VT12 by Pagani Geotechnical Equipment was used to measure the undrained cohesive strength of the soil as shown in **Figure 3.5**. The vane size with a diameter of 30 mm x 60 mm was selected for the test. The vane shear testing equipment consisting of torque wrench and different sized vanes is shown in **Figure 3.5.**

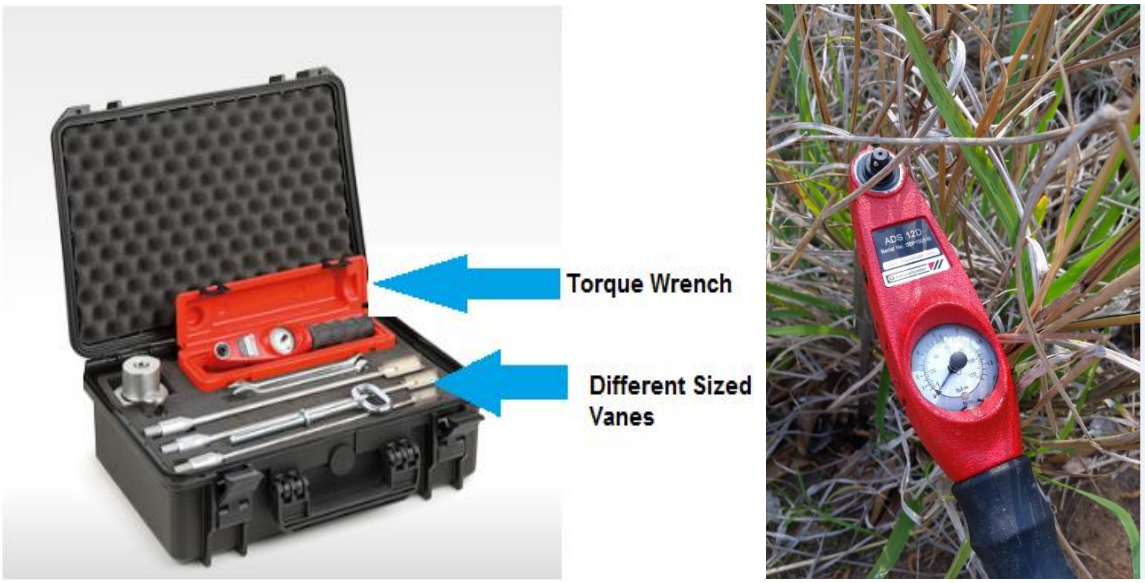

Figure 3.5: (left) Vane shear testing equipment box with a torque wrench and three different sized vanes; (right) Vane shear test machine being used in the field.

The vanes were connected through rods to the torque wrench, which measured the amount of torque applied to the soil in the ground at different depths. Tests were done on three different locations of each of the Cycle 1 and Cycle 3 of the CS-28 project. ASTM D2573 standard was used to determine the peak undrained shear strength of the soil.

Tests were done to a depth of 40 cm, assuming that to be the maximum depth the roots of *Spartina alterniflora* can reach. Vertical profiles of vane shear strength were made at 10-cm increments at each of the testing locations. The soil was considered undrained and it was assumed that no consolidation took place while inserting the vane or during the test. Isotropic strength conditions were assumed to exist in the soil mass. The remolded zone around the vane was assumed to be very small.

The un-drained shear strength of soil (S_u) was calculated using **Eq. 3-1**:

$$S_u = \frac{T}{\pi\left(\frac{d^2h}{2} + \frac{d^3}{6}\right)} = \frac{6T}{7\pi d^3} \ (for\ h = 2d) \qquad \textbf{Eq. 3-1}$$

where T is the maximum torque reading, which is noted on the torque wrench, h is the height of the vane and d is the diameter of the vane. The equation also shows that for a vane with a height-to-diameter ratio of two, shear resistance on a vertical plane produces a torque of magnitude six times than that on the horizontal planes.

Undrained shear strength calculated from the field vane test should be corrected to account for factors like anisotropy, strain effects, and disturbance. Based on computed factors of safety (FS) with known field vane shear strength, Bjerrum (1972) calculated the correction factor (μ) which is defined by **Eq. 3-2** as:

$$\mu = \frac{1}{FS} = 1.7 - 0.54\, log(PI) \qquad \textbf{Eq. 3-2}$$

where PI is the plasticity index of the soil. **Eq. 3-2** is used in this study to calculate the corrected vane shear strength. It is plotted in **Figure 3.6.**

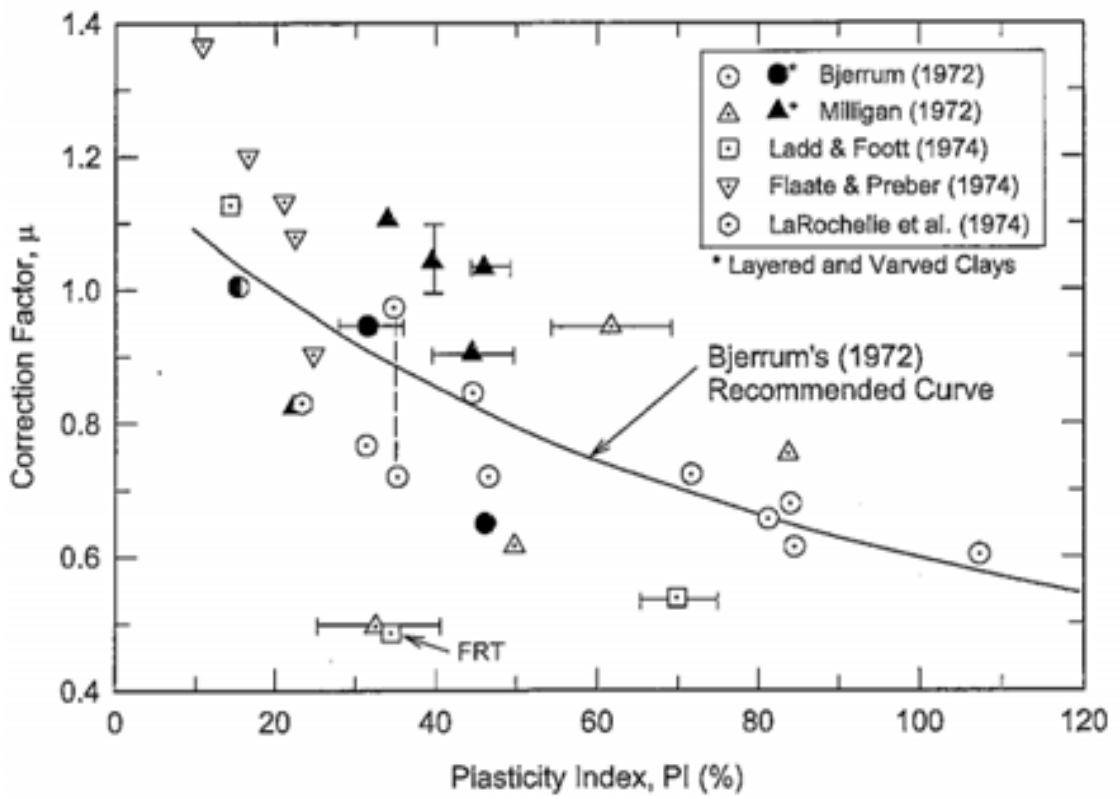

Figure 3.6: Bjerrum's (1972) recommended curve to calculate the correction factor for calculated undrained shear strength by Vane Shear Test.

After the vane shear test, undisturbed soil samples were collected using Shelby tubes and PVC core samplers. The collected soil samples were stored in airlock bags to preserve the moisture and they were brought to the soil testing lab for further testing. Although the cone penetration test was tried at all the sampling locations, no results were obtained from the digital penetrometer used. It was because the soil was very soft to provide any resistance to the tip of the penetrometer. In addition to the un-disturbed samples, disturbed samples were also obtained from each *in-situ* location for soil characterization and for the measurement of water content. Disturbed soil samples were also stored in airlock bags. **Figure 3.7** shows the different process of *in-situ* tests and soil sample extraction.

Figure 3.7: (left) Using extruding rod with hammer to get soil samples from Shelby tube from inside the quadrant as seen in picture; (mid) Trimming soil samples at different depths obtained from PVC core sampler; (right) Penetrometer test being conducted on the site.

3.4 Lab Tests

This section provides the description of the instruments used and methodology to conduct laboratory tests of soil specimen and root samples collected from the site.

3.4.1 Atterberg's Limit Test

Liquid limit is defined as the water content when the soil changes from plastic stage to liquid stage. ASTM D4318 was followed to measure the liquid limit of the soil obtained from the site. **Figure 3.8** shows the arrangement of the liquid limit test in the lab.

Figure 3.8: (left) Equipment required to conduct the liquid limit test including the Casagrande's apparatus; (right) Groove cut at center of brass cup using a grooving tool.

Plastic limit is defined as the moisture content when the soil changes from plastic state to semi-solid state. It is the moisture content when the soil just begins to crumble when rolled into a thread of 1/8 inches. ASTM D4318 was followed to measure the liquid limit of the soil obtained from the site. **Figure 3.9** shows the arrangement of the plastic limit test in the lab.

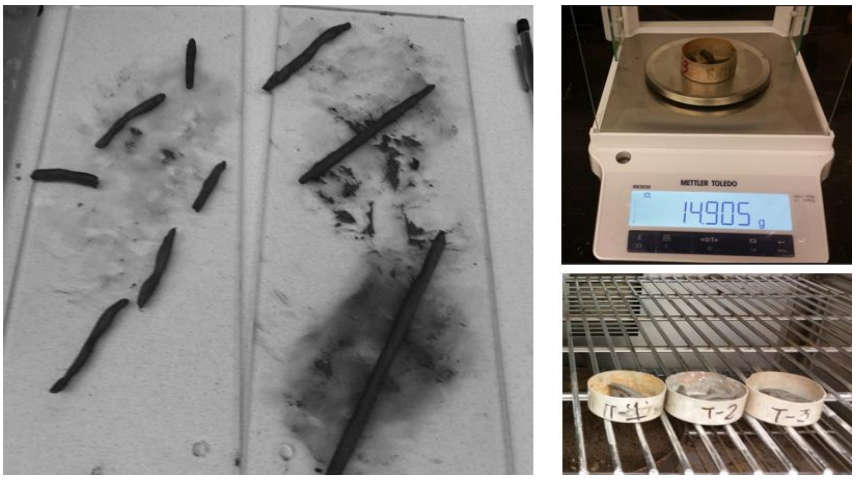

Figure 3.9: (left) Soil rolled till they crumbled in threads of size 1/8" on glass plate; (top right) Weight measurement of crumbled soil masses with the precision of three decimal places; (bottom right) Oven drying the cans to obtain moisture content.

3.4.2 Direct Shear Test

Undisturbed soil samples collected from sites using the Shelby tubes were first extruded by a hydraulic extruder. Sufficient care was followed to ensure undisturbed condition while extruding and preparing the soil samples. A minimum of four soil specimens was obtained from each of the Shelby tubes. Using the soil cutter, uniform soil specimens were prepared with diameter of 63.5 mm and height of 20 mm. Soil samples were then labeled according to their depths and locations. After taking the initial measurements, these specimens were then transferred to shear box where they were sandwiched between wet porous stones. Soil specimen were classified in three layers depending upon the depth of the specimen from the ground surface. The three layers were designated as Layer 1 (0 - 8 cm), Layer 2 (8 cm – 16 cm) and Layer 3 (16 cm - 24 cm). Soil samples below the depth of 24 cm hardly had any live roots. So, the soil samples collected below these depths were assumed to be plain soil not having any roots of *Spartina alterniflora*.

A total of twenty-four soil specimens were prepared for direct shear tests, twelve from each of Cycle 1 and Cycle 3 at the CS-28 project site. For each layer at least three soil specimens were tested to help obtain strength parameters of the soil; i.e., cohesion (c) and friction angle (ϕ).

Direct shear tests were performed in Louisiana Tech's Geotechnical Engineering Laboratory using the ELE International Direct shear test machine as shown in **Figure 3.10**. ASTM D3080 was followed for the direct shear tests. Consolidated drained direct shear test was performed on rooted and non-rooted soil samples collected from the site. The testing was controlled using "Data-System 7 (DS7)" software developed by ELE

International. The software provides automatic data acquisition, real-time data display, and information regarding details and procedure of the test. It can also be used to control several tests at the same time and to generate test reports at the end of a test.

Figure 3.10: The ELE international Direct Shear Machine.

ELE international direct shear test machine consists primarily of a direct shear box, which can be split into two halves and holds the specimen; a load cell to measure the force acting on the specimen, horizontal and vertical transducers to measure the deformation in respective directions; and a lever-hanger system which multiplies the vertical load applied on the specimen by a ratio of 10:1. A controlled horizontal load was applied using a motor and gear arrangement system. In this research, strain-controlled tests were used. To maintain a drained condition and make the pore water pressure (u) zero, a very small rate of strain equaling 0.1 mm/min was applied on the upper half of the shear box during the shearing stage of the test. The detailed process of a direct shear test

is illustrated in **Figure 3.11 (**Process for direct shear test starts from step “a” and ends at step “g”).

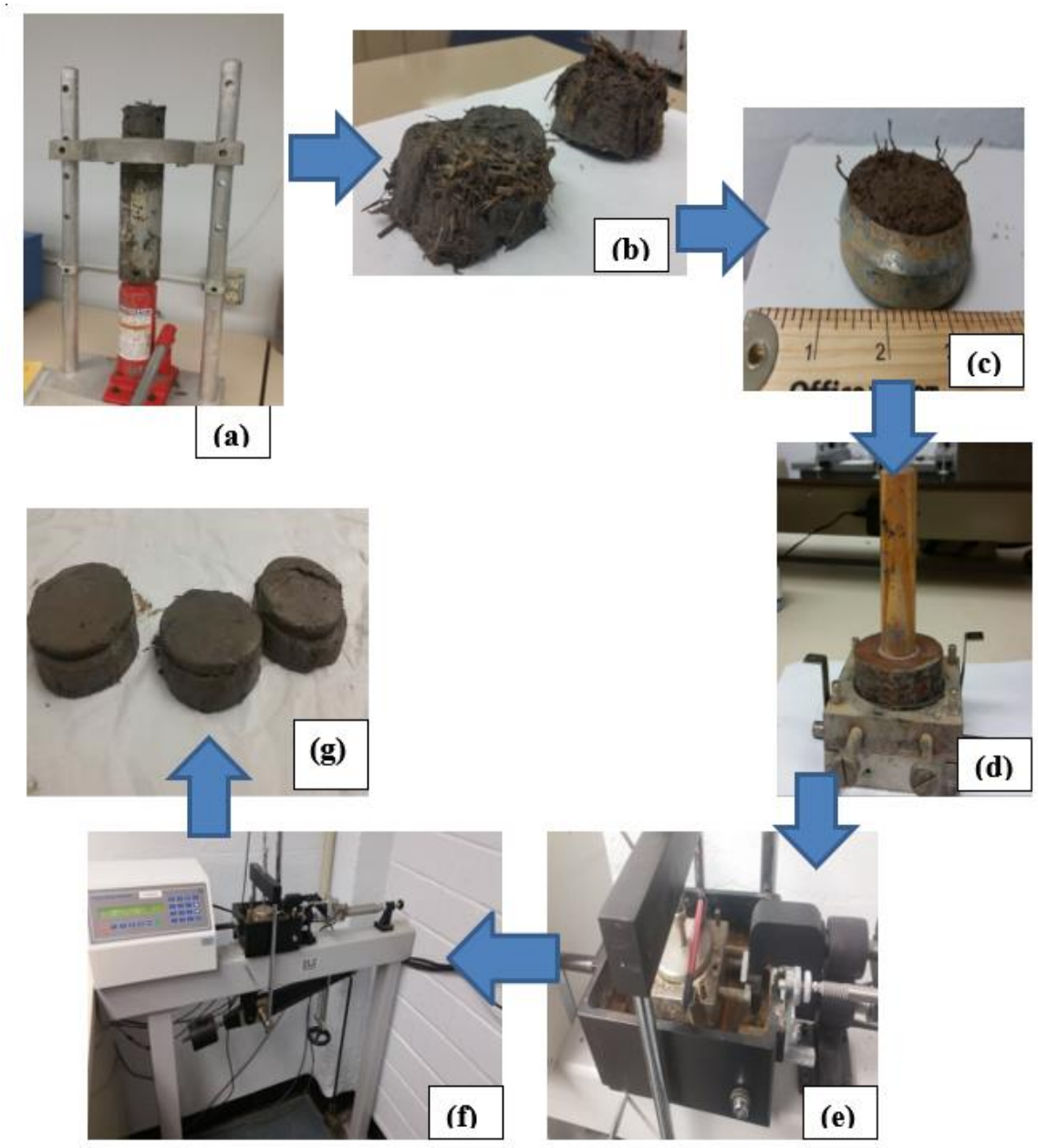

Figure 3.11: (a) Undisturbed soil samples being extruded from Shelby tubes, (b) Rooted soil samples cut according to depths, (c) Rooted soil sample trimmed by cutter, (d) trimmed soil samples pushed inside the shear box, (e) Shear box transferred to Direct Shear Machine, (f) Direct Shear Machine during shearing phase, (g) Failed soil sample after the test showing distinct failure planes.

3.4.2.1 Consolidation Stage:

After mounting the shear box consisting of soil specimen onto the direct shear machine, the consolidation stage was started. Desired normal load to be applied on the specimen was obtained by hanging dead weight to a vertical load yoke and using the lever-hanger system which multiplies the vertical load applied to the specimen by a ratio of 10:1. Using the known area of the shear box, DS7 software computes the total normal stress acting on the specimen. Three different normal loads 5 kPa, 11 kPa and 19 kPa were selected. Once the desired normal stress was obtained, the screw which holds the weight on the yoke was released.

The normal load applied to the soil specimen causes a certain amount of compaction and dewatering, which results in gradual vertical settlement of the specimen. In an ideal situation, three distinct stages of consolidation are observed: an initial pre-compression period with a shallow slope, a primary consolidation period where the slope of the curve approaches a vertical line on the plot and a secondary consolidation period with a shallow slope (Braja 2008). DS-7 plots the graph as the test proceeds. Tests were stopped once a secondary shallow slope was established. **Figure 3.12** shows a typical consolidation curve (deformation vs square root minute) as plotted by DS-7 during this research.

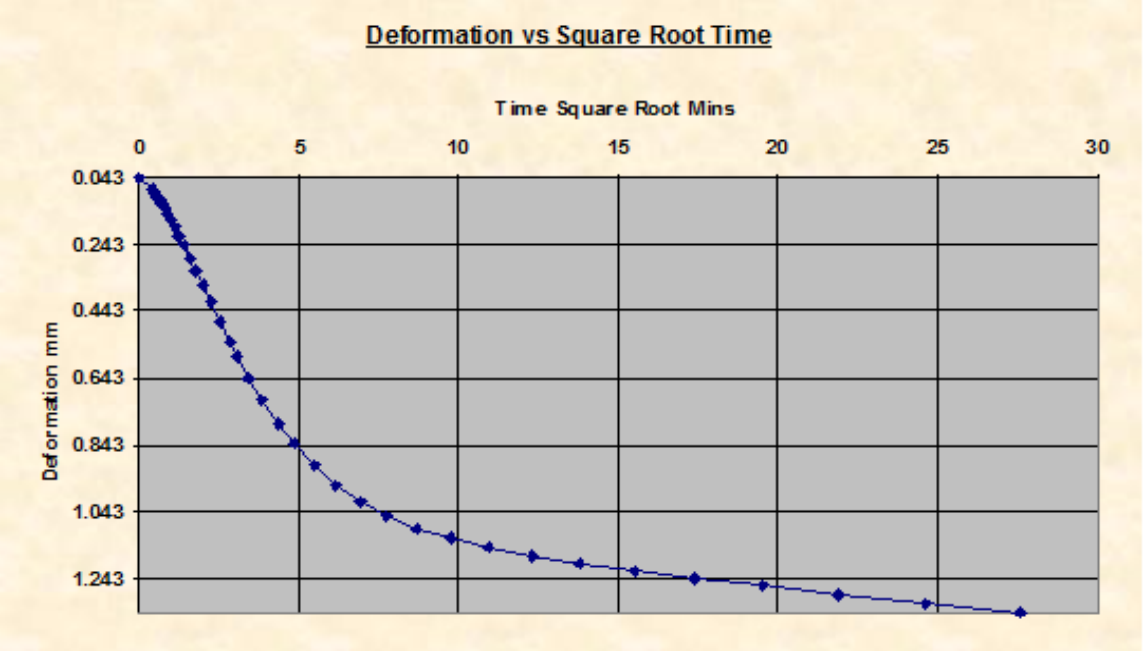

Figure 3.12: A typical consolidation curve obtained from DS-7 software during the consolidation stage of direct shear test.

3.4.2.2 **Shearing Stage:**

After the consolidation stage, vertical alignment screws that lock the two halves of the shear box were removed. A horizontal load was applied on the top half of the shear box using the gear and motor assembly. To ensure full drainage conditions and prevent pore pressure buildup, a slow rate of shearing equal to 0.1 mm/min was used. This rate was entered manually on the keypad of the direct shear machine and was kept constant in all the tests. As the test proceeded, a graph was plotted between shear stress acting on the soil sample and relative lateral displacement. The test was either stopped automatically or manually when a constant slope was obtained.

A typical shear displacement curve consisted of the increase in shear stress from zero to a maximum showing a high modulus of elasticity (E) in that period. Then for the same rate of the strain, the stress increase in a specimen is almost zero. After some

deformation, the shear stress will increase again but will have a relatively flatter slope. This process will either repeat or terminate in a straight-line graph with the shear stress becoming constant for any relative increase in displacement. This constant value was noted as the maximum shear stress acting on the specimen during failure. **Figure 3.13** shows the typical stress-displacement curve plotted by the DS-7 software.

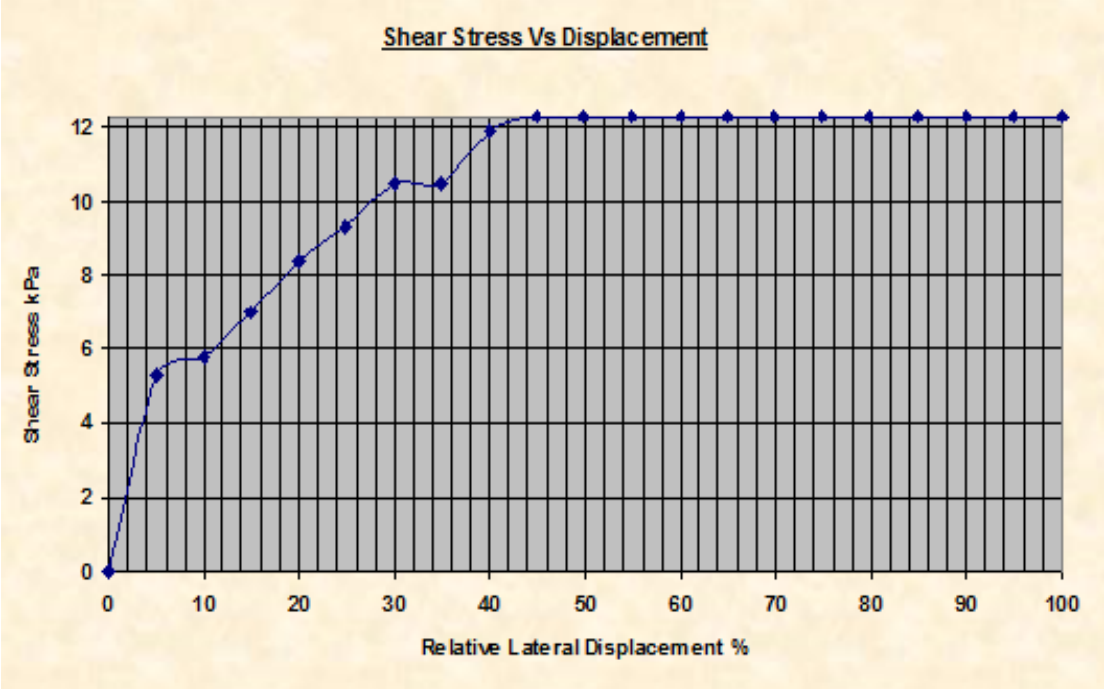

Figure 3.13: A typical shear vs. displacement curve obtained from DS-7 software during the shearing stage of direct shear test.

However, for the rootless soils, we could observe a sharp peak on the curve followed by a gradual decrease to a lower shear stress value that remains constant until the end of the test. This sharp peak was noted as the maximum shear strength of rootless soils.

Using the peak value of the shear stress and corresponding normal stress, a graph of shear strength versus normal stress (τ vs. σ) was plotted for all the tests which is illustrated in **Figure 4.6** and **Figure 4.10** of Chapter 4. For each soil layer, a minimum of three valid tests were done by varying the normal load. Value of cohesion (c) and angle of friction (ϕ) was obtained for each layer using these graphs. Line intercept of the graph gives the value of c and the slope of the line gives the value of ϕ.

3.4.3 Tensile Test

Tensile strength tests for the roots of *Spartina alterniflora* were conducted using the ADMET expert 2600 universal tensile testing machine at Louisiana Tech University. A low capacity load cell (667N) was used.

The root system of *Spartina alterniflora* was found adventitious in nature, which was composed of thicker underground stems or rhizomes and thinner fibrous roots. Rhizomes were found in shallow depths and their diameters decrease as they go deeper. Shoots and adventitious roots emerged from rhizome's nodes. Since shoots emerged from rhizomes, it was seen that, although plants appear to be distinctly individuals, in the ground they remain connected by rhizomes. Adventitious roots were found to grow almost perpendicular from rhizomes and were connected forming dense mesh at shallow depths. Unlike rhizomes, these roots have fine root hairs and can penetrate deeper into the soil.

The root system was classified into three major types depending upon their diameter sizes. The three root types are designated as: R_1 (0.16 inches - 0.22 inches), R_2

(0.06 inches - 0.15 inches) and R_3 (0.01 inches - 0.06 inches). **Figure 3.14** shows the three designated root types of *Spartina alterniflora*.

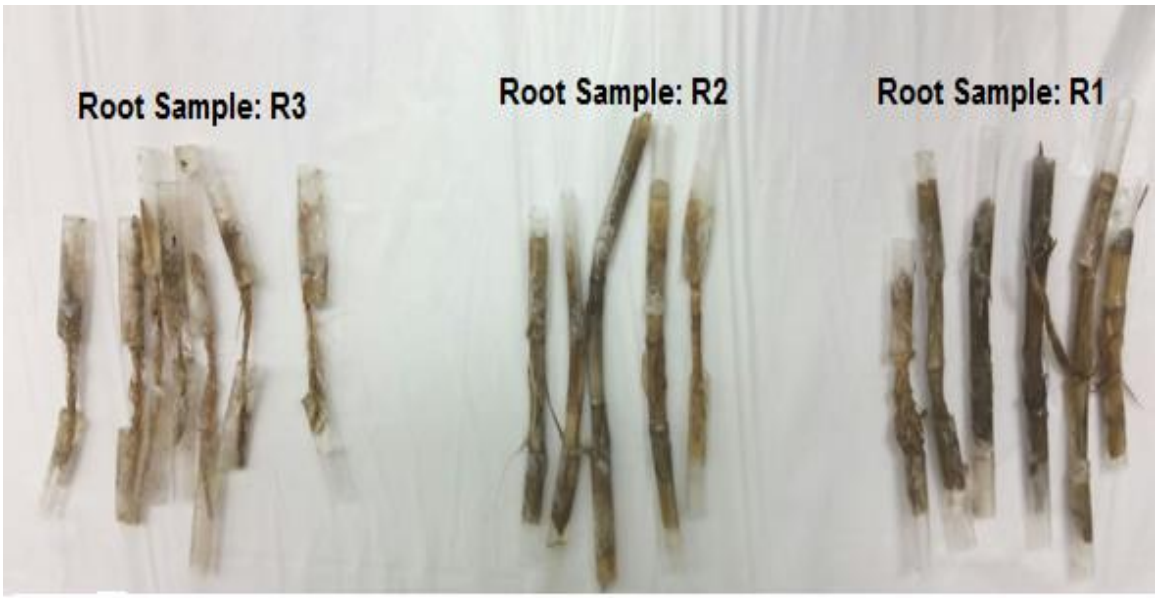

Figure 3.14: Three different root types of *Spartina alterniflora* showing their ends being prepared for the tensile test.

The diameters of all root specimen were measured at the middle and end of each piece using electronic slide calipers of 0.01 mm resolution. Root Area Ratio (RAR) is the ratio of the cross-sectional area of the soil covered by the roots per unit area (Gray & Leiser 1982). RAR values of *Spartina alterniflora* were found to decrease with the depth of the soil layer. To measure RAR representative soil samples from each layer were air dried in three separate cores of diameter 2.5 inches. Once the soil was air-dried, the soil samples were taken out from the core and were broken at the middle. Roots were then counted for each of the root types. Using the average diameter of each root type, RAR

was calculated as the fraction of the total root area by the total cross-sectional area of the soil core.

The main problem during the tensile test was found while clamping the ends of the root specimen. During each test, the root sample could easily slip out or break at the clamping points. This resulted in erroneous data and wastage of several valuable root specimen. After trying several methods, two different arrangement were finalized: Grip Arrangement (GA) and Hook Arrangement (HA). **Figure 3.15** shows the experimental set up for the GA and HA methods, respectively.

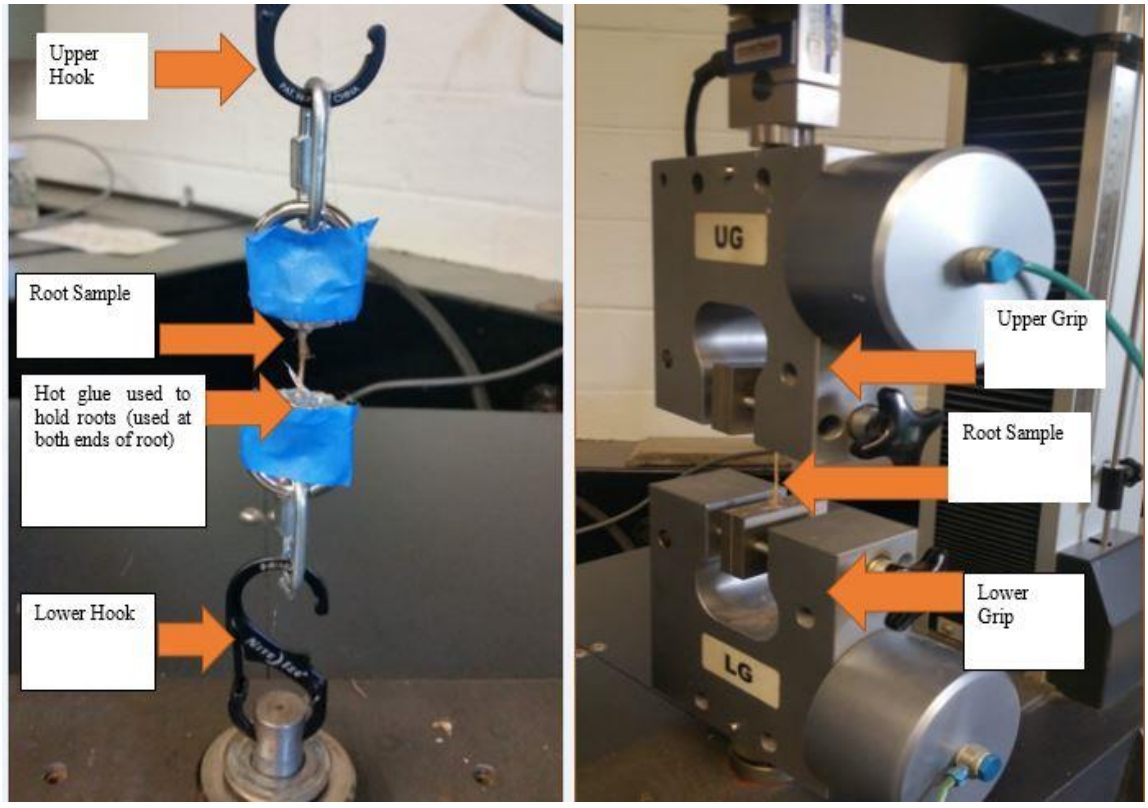

Figure 3.15: (left) Hook arrangement for tensile test showing hooks, root samples and parts consisting of hot glue to hold the root sample; (right) Pneumatic grip arrangement showing upper and lower grips and root sample.

Pneumatic grips were used in the GA method to hold and pull the roots at both ends. Root ends were covered with hot glue which prevented the slipping of roots and protected it from crushing from pressure of pneumatic grips. In the HA method, hooks were used to hold the root specimens using hot glue and double round eye swivel. For both arrangements, the tests were considered invalid if the failure occurred at the clamping ends. A total of thirteen valid test results was obtained at the end of several root tensile tests. GA was used to test root type R_1 with bigger diameters and HA was used to test root types R_2 and R_3 of relatively smaller diameters.

Root diameter was measured using digital electronic slide calipers of 0.01 mm resolution as shown in **Figure 3.16**. The test was conducted with a constant loading rate and the test specimens were cut to an equal length of 2 inches to maintain uniformity.

Figure 3.16*:* Electronic slide caliper used to measure the root diameters of *Spartina alterniflora*.

A uniform distance of one inch was established between the two pneumatic grips or hooks. **Figure 3.17** illustrates the initial set up for the HA test and **Figure 3.18** shows the failed root sample after the root tensile test, which indicates that the test failed.

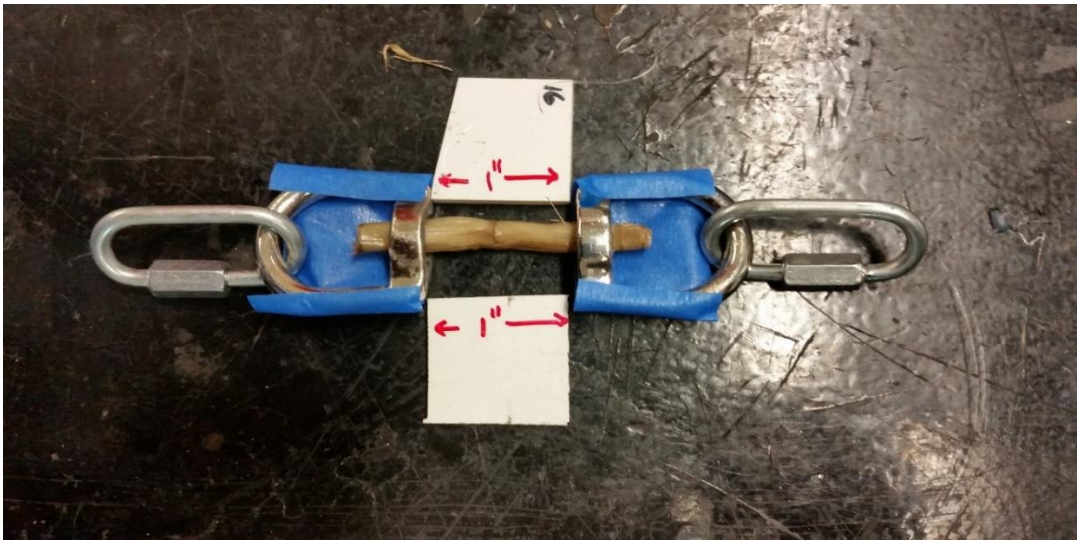

Figure 3.17: Tensile test set up using Hook arrangement before pouring hot glue at the ends of double round eye swivel (wrapped by blue tape at the bottom).

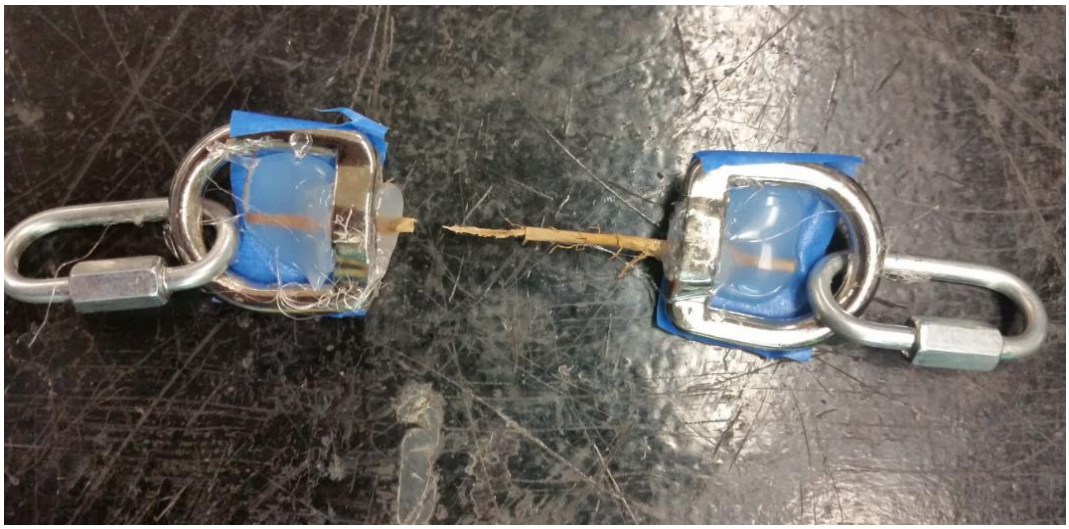

Figure 3.18: Failed root sample after the test showing the stretched inner vascular membranes.

3.4.4 Below Ground Biomass Measurement

Two methods were used to measure the belowground biomass. For the first method, the soil sample after the direct shear test was air-dried to obtain the total dry weight. Then the dried soil sample was washed (i.e. wet sieving) through two sieves with a mesh size of 0.6 mm (sieve no. 30) and 0.25 mm (sieve no. 60), respectively, to separate roots from the soil as shown in **Figure 3.19.** After the wet-sieving, the roots were air-dried to obtain the weight of dry roots. A minimum of two samples from each layer were wet sieved and roots were air dried as shown in **Figure 3.20**. The weight of the roots was measured using a sensitive balance to 3 decimal places. Finally, the root content was calculated using **Eq. 3-3**.

$$\text{Root content} = \frac{\text{Weight of the dry roots}}{\text{Weight of the dried soil sample}} \qquad \textbf{Eq. 3-3}$$

Figure 3.19: (left) Wet washing the roots in sieve nos. #30 and #60 to separate roots from the soil; (right) Representative soil samples used to measure the underground biomass (two samples for each layer).

Figure 3.20: Air-drying the root samples (two from each soil layer) collected from wet sieving.

As for the second method, a representative soil sample for the given layer was left to air dry. Later, the soil sample was broken from the middle and the number of roots present in the cross-section was counted as shown by **Figure 3.21**. The number of roots were counted for each of the root types. For each root type, an average diameter was used, and the total root area was counted. With the known cross-sectional area of the soil sample, the root area ratio (RAR) was calculated using the formula:

$$RAR = \frac{\sum_{i=1}^{n} A_{ri}}{A} \qquad \textbf{Eq. 3-4}$$

where "*i*" represents the i^{th} single root, A_{ri} is the area of the i^{th} root, A is the total cross-section area of the soil sample, and n is the total root number.

Figure 3.21: (left) Soil cores of each layer with roots of *Spartina alterniflora* let to air dry in the lab; (right) Broken soil core showing the roots of the plant.

3.5 Delft3D

QUICKPLOT, a post-processing tool of Delft3D was used to extract the results from a validated WAVE-FLOW coupled model with Hurricane Ike forcing condition to investigate the mass erosion that happened at the marsh creation project site CS-28. Results analysis were done for four scenarios with different grid conditions (Shariar 2017). They are:

1. Submerged grid condition without vegetation
2. Dry grid condition without vegetation
3. Submerged grid condition with vegetation
4. Dry grid condition with vegetation

Sampling location where *in-situ* tests was done were located by matching the M-value from Delft3D GRID with the known longitudes of the sampling station and by matching N- value from Delft3D GRID with the known latitudes of the sampling station.

First, for the known value of latitude of a sampling station, the corresponding value of N was located from Delft3D GRID as shown in **Figure 3.22**.

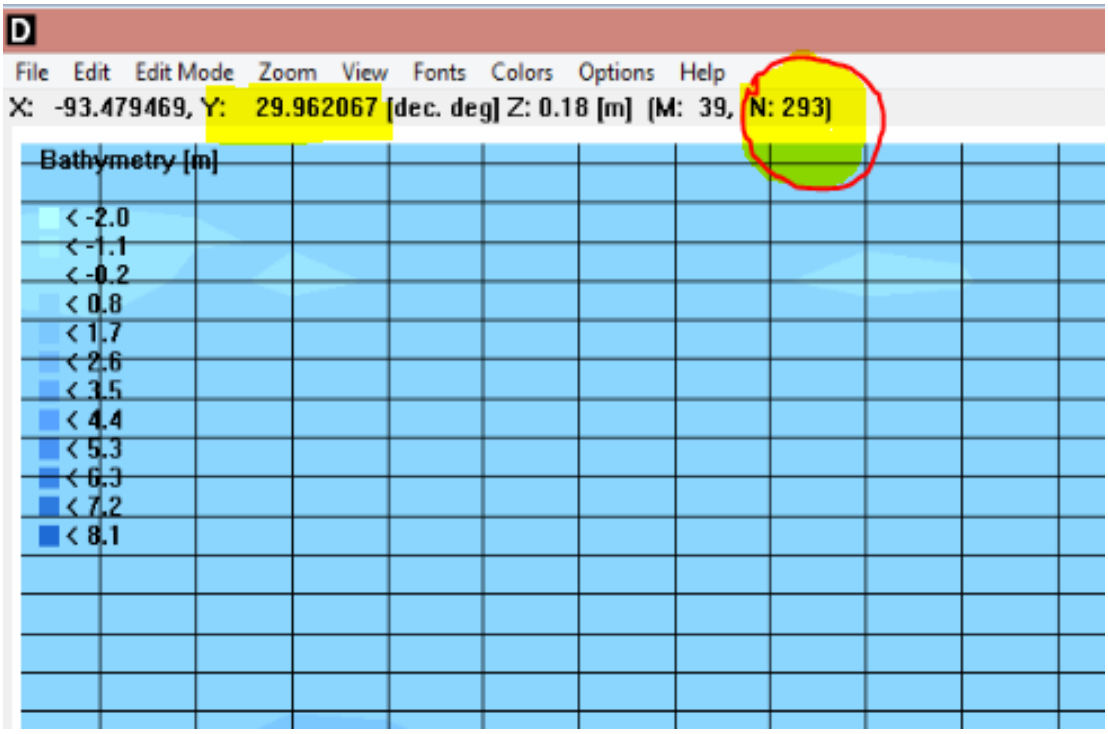

Figure 3.22: A screenshot of Delft3D GRID showing the N value for the corresponding latitude of a sampling location.

Out of the two extreme periods during the Hurricane Ike, Land Fall on September 12 at 18:00 hours and Peak Surge on September 13 at 2:00 hours (Shariar 2017), analysis was done for Peak Surge period. It was because the value of bed shear stress and water velocity was found higher during this time period. **Figure 3.23** shows a screenshot of Delft3D QUICKPLOT showing the selected time of peak surge and the corresponding N value of a sampling station to plot the maximum bed shear stress for that location.

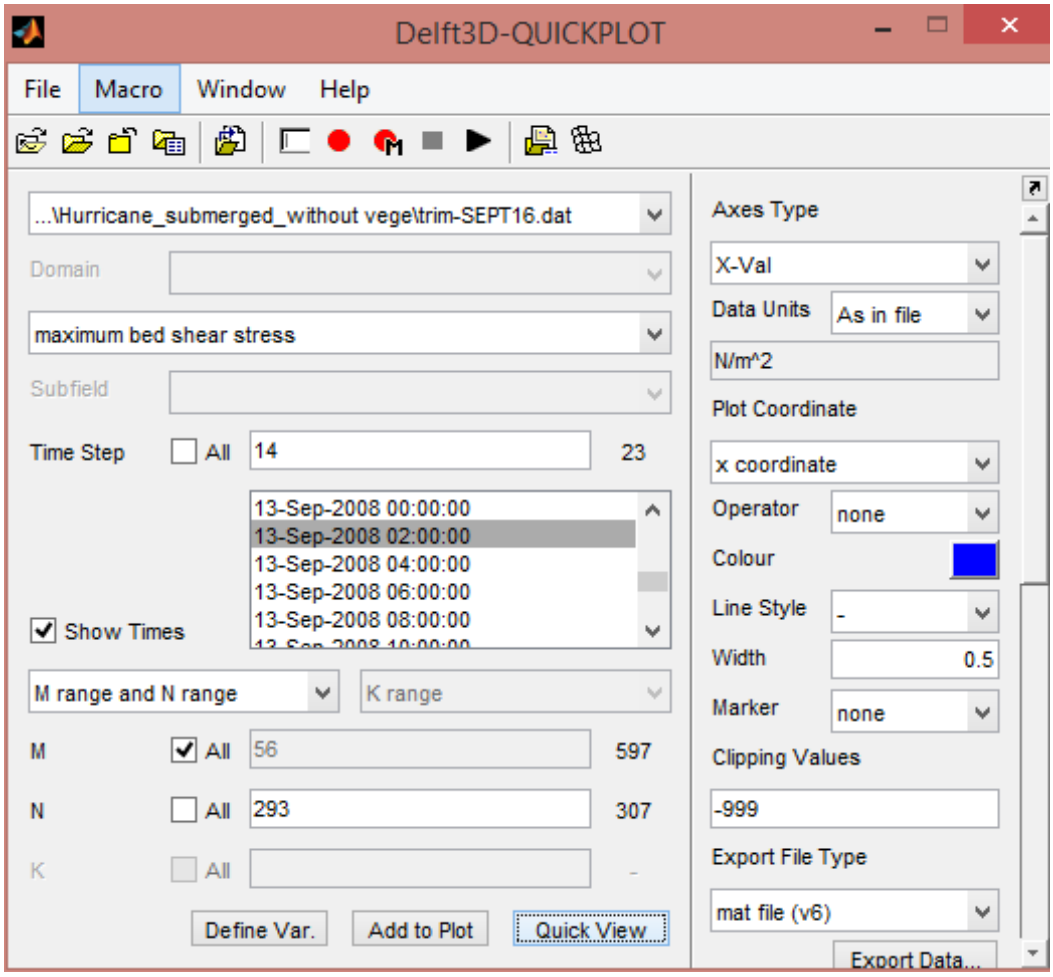

Figure 3.23: A screenshot of the QUICKPLOT, showing the selected time of the peak surge and N value equal to 293 for a sampling location.

With the selected value of time and the N value, QUICKPLOT was used to plot the graph of the required parameter. **Figure 3.24** and **Figure 3.25** show the plot of the maximum bed shear stresses and the magnitude of wave velocity respectively, for the selected value of N.

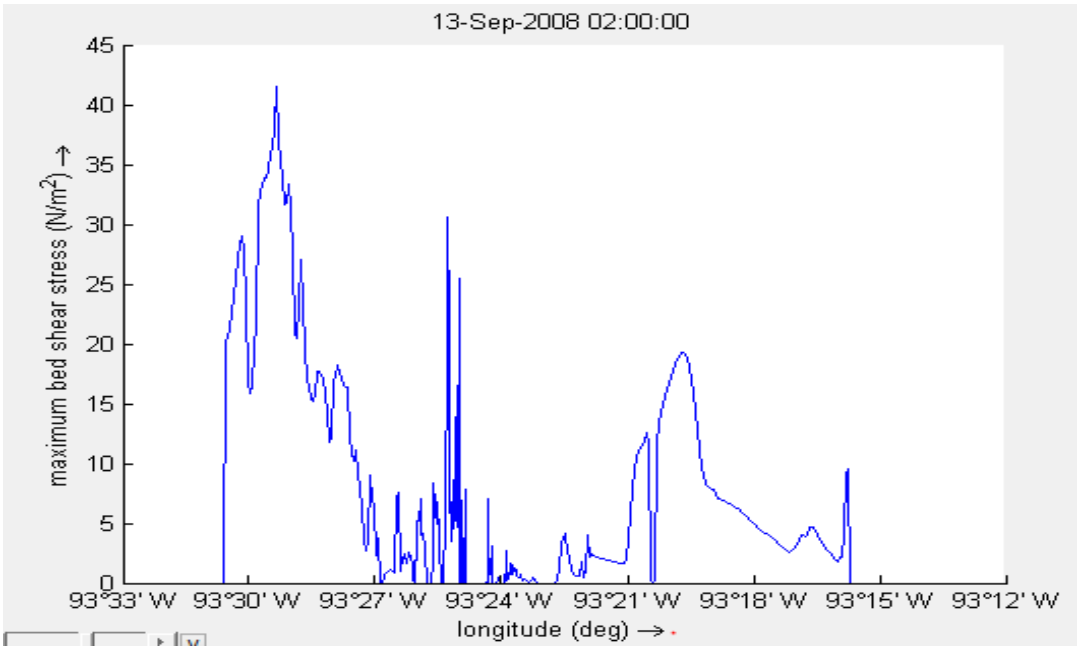

Figure 3.24: A graph of the maximum bed shear stress obtained from post processing tool, QUICKPLOT, for the entire range of M (longitude) and a specific value of N.

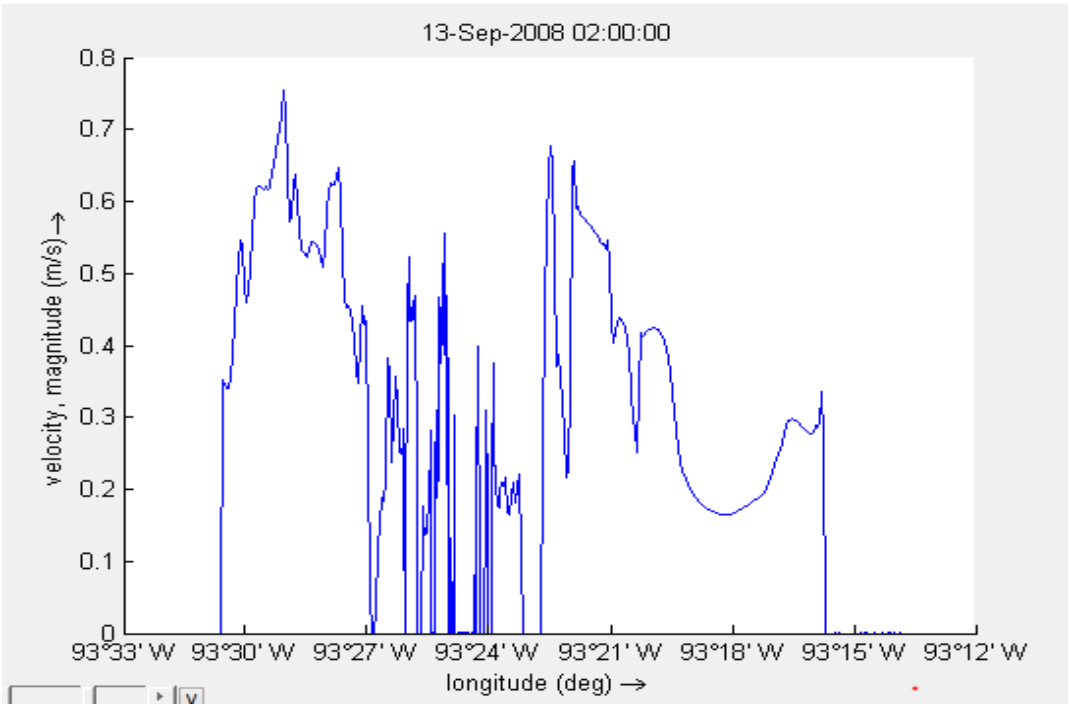

Figure 3.25: A graph of magnitude of wave velocity obtained from post processing tool, QUICKPLOT, for the entire range of M (longitude) and a specific value of N.

After plotting these graphs, the required value of the maximum bed shear stress and the maximum wave velocity was obtained for the specific location. The same process was followed to obtain the value of the maximum bed shear stress and the maximum wave velocity for all the sampling stations. This method was followed for each of the four different grid conditions.

CHAPTER 4

RESULTS AND DISCUSSIONS

This chapter presents the overview of the results of all tests done in the soil sample of Cycle 1 and Cycle 3 of CS-28 project in Sabine Refuge M Marsh creation project in Louisiana. It includes the results of *in-situ* tests, lab tests, analytical model tests and finite element analysis study.

4.1 Vane Shear Tests

The correction factor (μ) was calculated using the Bjerrum's formula given by Equation 8. It was found to be equal to 0.9 for the soil with plasticity index of 32.4%. The resulting corrected undrained shear strength profile of the soil at different locations of Cycle 1 and Cycle 3 of the CS-28 project is shown in **Figure 4.1**. Undrained shear strength (S_u) of the soil was highest at the ground level, and it decreased with the depth. Overall, "Station 2" of Cycle 1 had the highest value of S_u and "Station 1" of Cycle 3 had the lowest value of S_u. At the ground level, undrained shear strength was found to be higher with a range of 6.82 kPa to 10.45 kPa. It is because of the presence of a large number of rhizomes and adventitious roots present in the top soil layer which contributed to large amount of reinforcement to the soil. S_u decreased highly to the range of 5.5 kPa to 7.5 kPa at the depth of 10 cm from ground. The decrease in undrained shear strength was because of the decrease in the number of roots with increasing depth. Value of S_u was comparable at depths of 30 cm and 40 cm. It is because there is very little presence

of roots at those depths. At a depth of 40 cm, value of S_u was the lowest where it ranged from 3.18 kPa to 4.54 kPa.

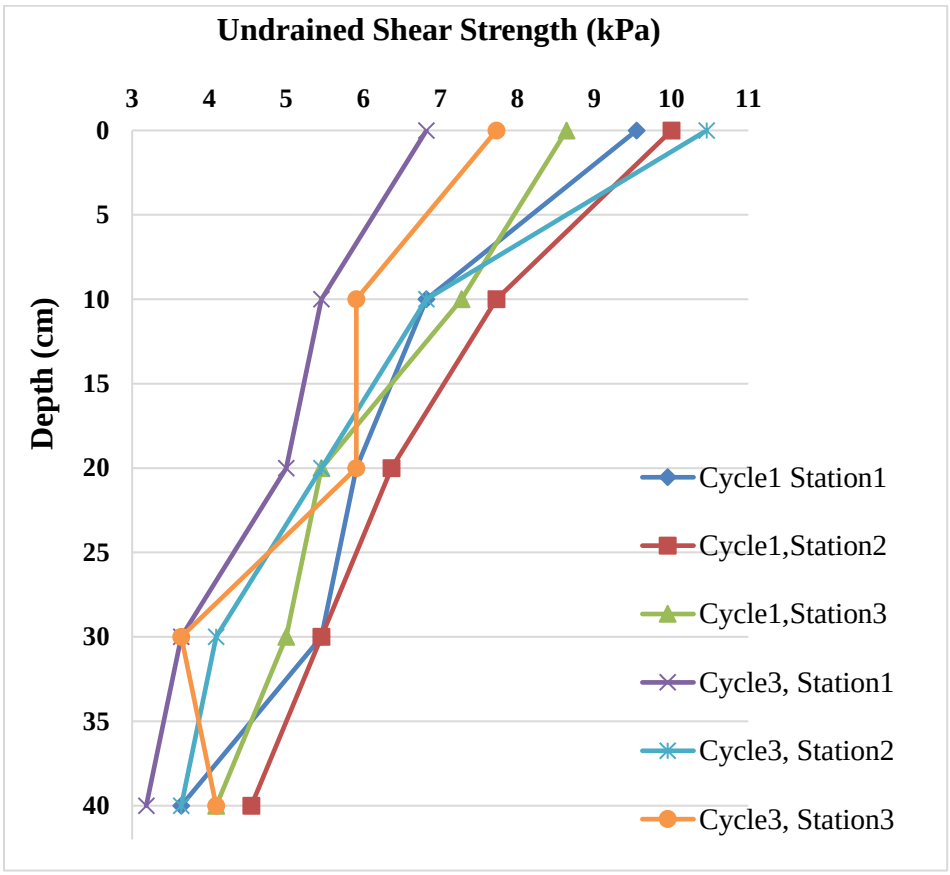

Figure 4.1: Corrected undrained shear strength profile obtained from Vane Shear Test for six different locations at the CS-28 project.

4.2 Tensile Strength Test of Roots

Root type "R_1" with mean diameter of 4.572 mm (0.18 inches) had the highest peak load value at failure which ranged from 28.168 N to 42.675 N. Root type "R_3" with the mean diameter of 0.762 mm (0.03 inches) had the lowest peak load value which ranged from 5.429 N to 8.7665 N. However, when this load was proportioned depending

upon the root diameter, it can easily be seen that lateral roots "R_3" can support a relatively higher peak load than R_1. Since the root area ratio (RAR) was calculated using the average diameter of each root type, the tensile strength was also calculated for average root diameter for each of the root type. The average diameter for root type R_1, R_2 and R_3 were 0.18 inches, 0.1 inches, and 0.03 inches, respectively. Average tensile strength was 2.24 MPa, 2.55 MPa, and 15.72 MPa for root types R_1, R_2 and R_3 respectively as shown in **Table 4.1**.

Table 4.1: Peak load, average root diameter, tensile strength and averaged tensile strength of roots of *Spartina alterniflora*.

Root Type	Root Sample	Peak Load(N)	Avg. Dia. (mm)	Tensile Strength (kPa)	Avg. Tensile Strength (kPa)
R1	R11	42.658	4.572	2598.381	2244.34
	R12	39.722	4.572	2419.556	
	R13	28.157	4.572	1715.094	
R2	R21	16.592	2.54	3274.45	2553.13
	R22	9.519	2.54	1878.64	
	R23	8.496	2.54	1676.73	
	R24	15.747	2.54	3107.65	
	R25	14.679	2.54	2896.96	
	R26	12.588	2.54	2484.37	
R3	R31	8.185	0.762	17947.53	15720.34
	R32	7.918	0.762	17362.28	
	R33	7.073	0.762	15509	
	R34	5.649	0.762	12387.69	
	R35	5.427	0.762	11899.99	
	R36	8.763	0.762	19215.56	

Figures 4.2, 4.3 and **4.4** show the load-deformation curve for different root samples. **Figure 4.5** shows the exponential increase in root tensile strength as the root diameter decreased. **Figure 4.5** also shows the higher variability of tensile strength of

small roots when compared to large roots. The value of α and β, calculated using **Figure 4.5** and **Eq. 2-5** (Gray & Sotir 1996)**,** was equal to 10.153 and 1.23 respectively. These values can be used for preliminary estimation of tensile strength of *Spartina alterniflora* for the known value of root diameter.

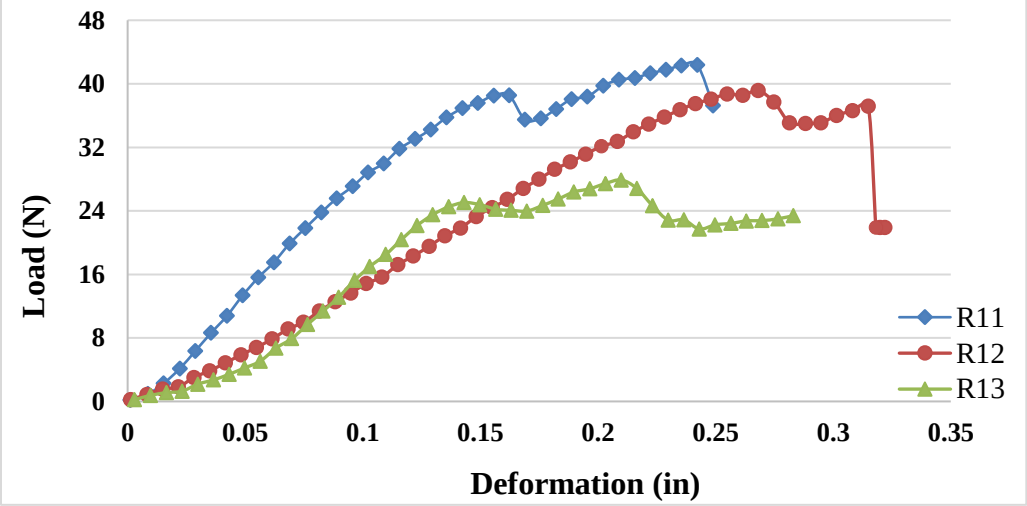

Figure 4.2: Graph of load vs. deformation for different root samples of root type "R_1".

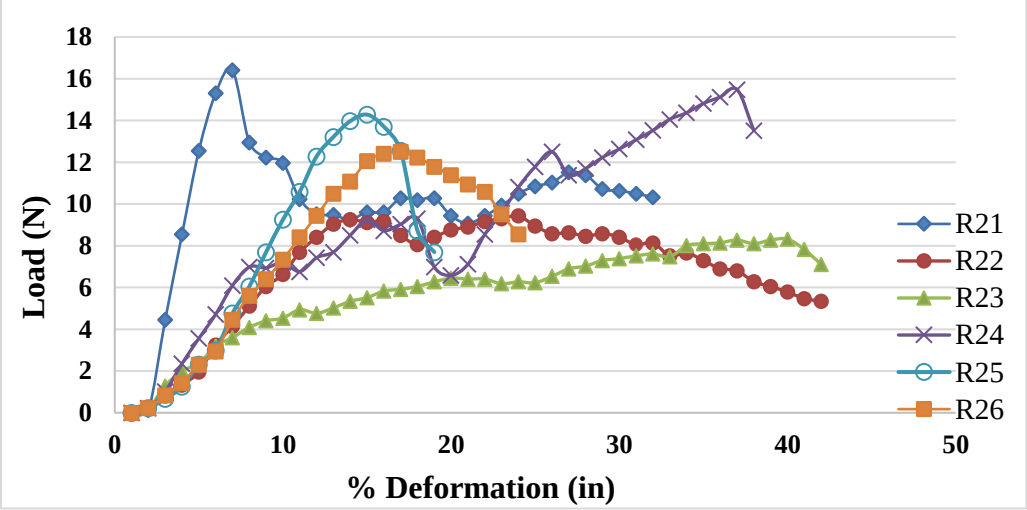

Figure 4.3: Graph of load vs. percentage lateral deformation for different root samples of root type "R_2".

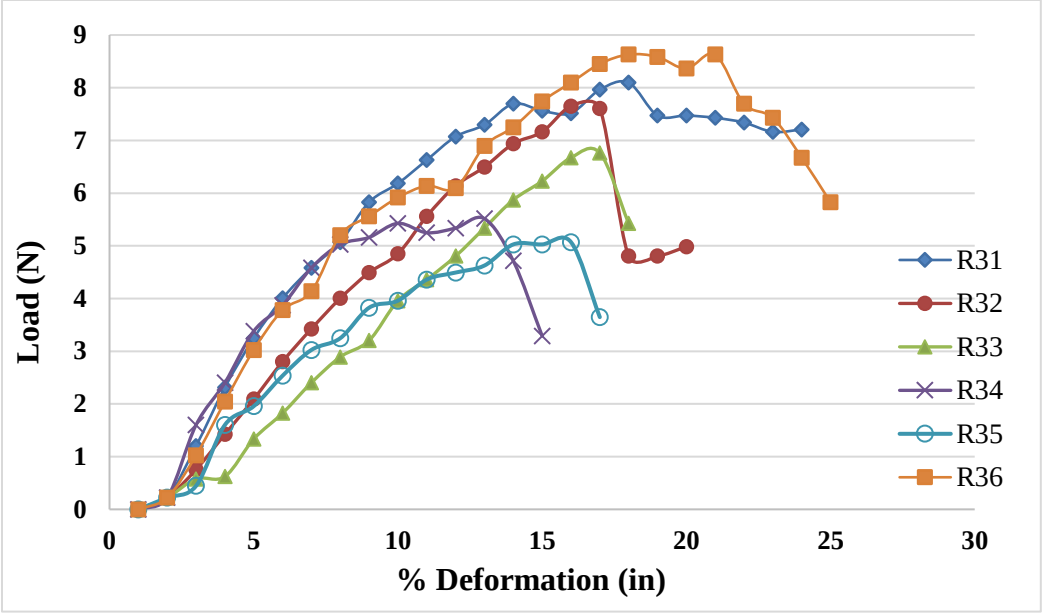

Figure 4.4: Graph of load vs. percentage lateral deformation for different root samples of root type "R_3".

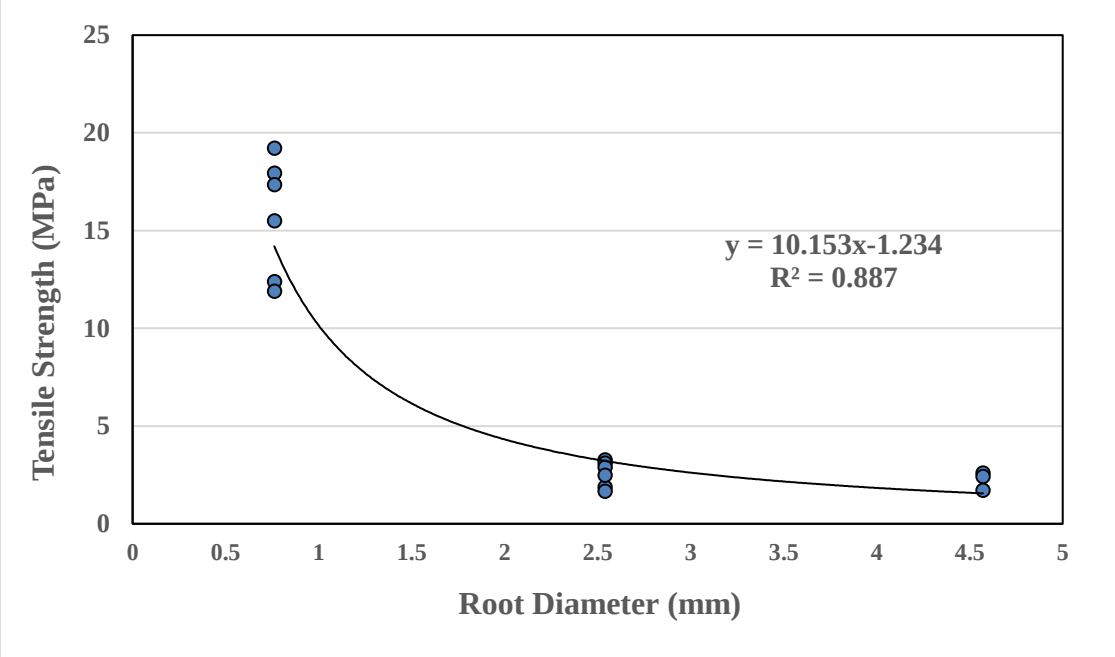

Figure 4.5: Graph of root tensile strength (MPa) vs. root diameter (mm) showing the power law regression.

4.3 Direct Shear Tests

For Cycle 1 of CS-28 project site, highest and lowest value of cohesion (c) was found equal to 5.51 kPa for Layer 1 and 2.48 kPa for "Plain Soil Layer" respectively as shown in **Table 4.2**. It was found that peak shear strengths were increased for all the rooted soil samples. The value of peak shear strength was found to be decreasing with depth increments. Reinforcement provided by the roots increased cohesion of soil by approximately 130% for Layer 1, 70% for Layer 2 and 12.5 % for Layer 3. The result shows that there is a high influence of root reinforcement till the depth of 24 cm after which there is negligible increase in root cohesion. Unlike the study shown by Wu *et al*. (1979) which suggested that there is no contribution of roots in soil friction angle, it was found that the presence of roots significantly increases the friction angle of a soil layer.

Table 4.2: Calculation of values of cohesion (c) and friction angle (ϕ) for different soil layers of Cycle 1.

Normal Stress (kPa)	**Peak Shear Strength (kPa) for Cycle 1**			
	Layer 1 (0-8cm)	Layer 2 (8-16 cm)	Layer 3 (17-24 cm)	Plain Soil (no roots)
5	9.02	7.24	5.43	3.62
11	14.54	9.04	6.03	5.43
19	19.80	14.54	10.9	7.15
Cohesion (c) (kPa)	5.51	4.08	2.75	2.48
Friction Angle (ϕ)	37.40°	27.80°	21.93°	14.04°

Figure 4.6 shows the Mohr's failure envelope of soil at different depths in Cycle 1 of the CS-28 project**. Figures 4.7, 4.8** and **4.9** show the stress-strain curve of soil layers in Cycle 1 for different normal load value of 5 kPa, 11 kPa, and 19 kPa, respectively.

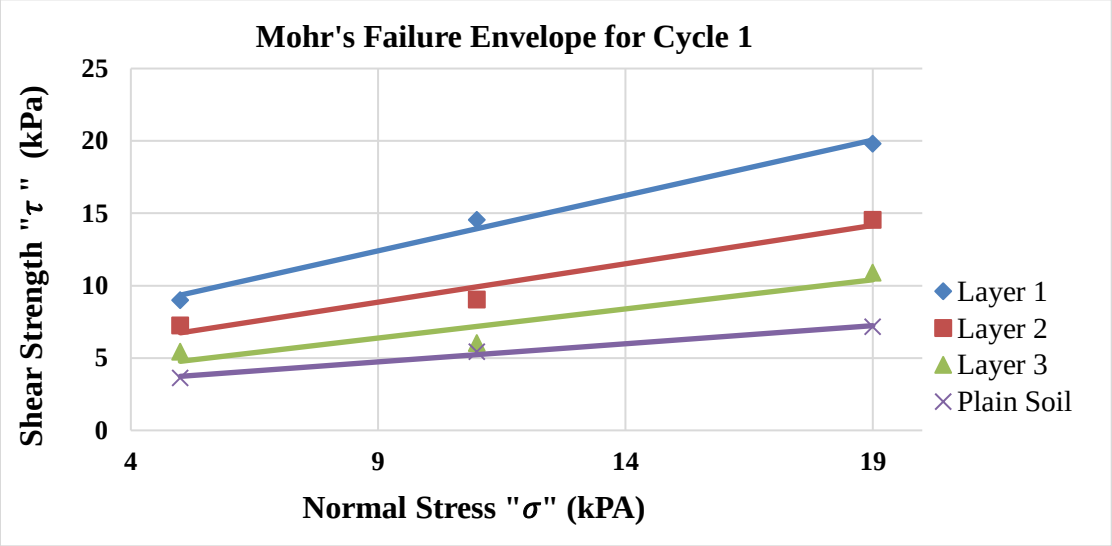

Figure 4.6: Graph of normal stress vs. shear strength for soil samples from Cycle 1 of CS-28 project.

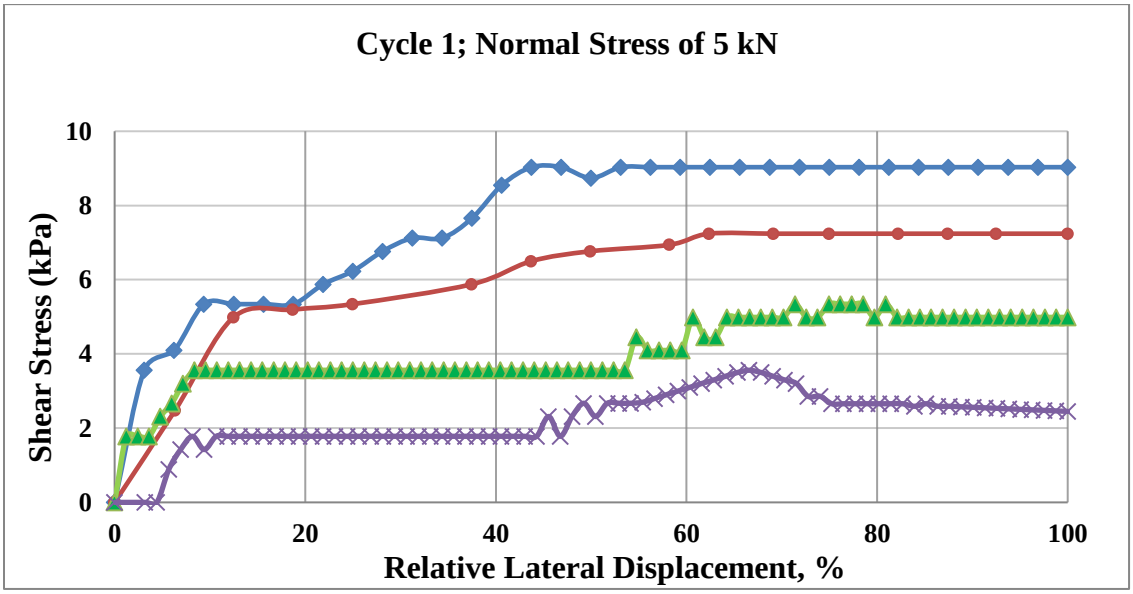

Figure 4.7: Stress-Strain curve for soil samples from Cycle 1 for a normal stress of 5 kN.

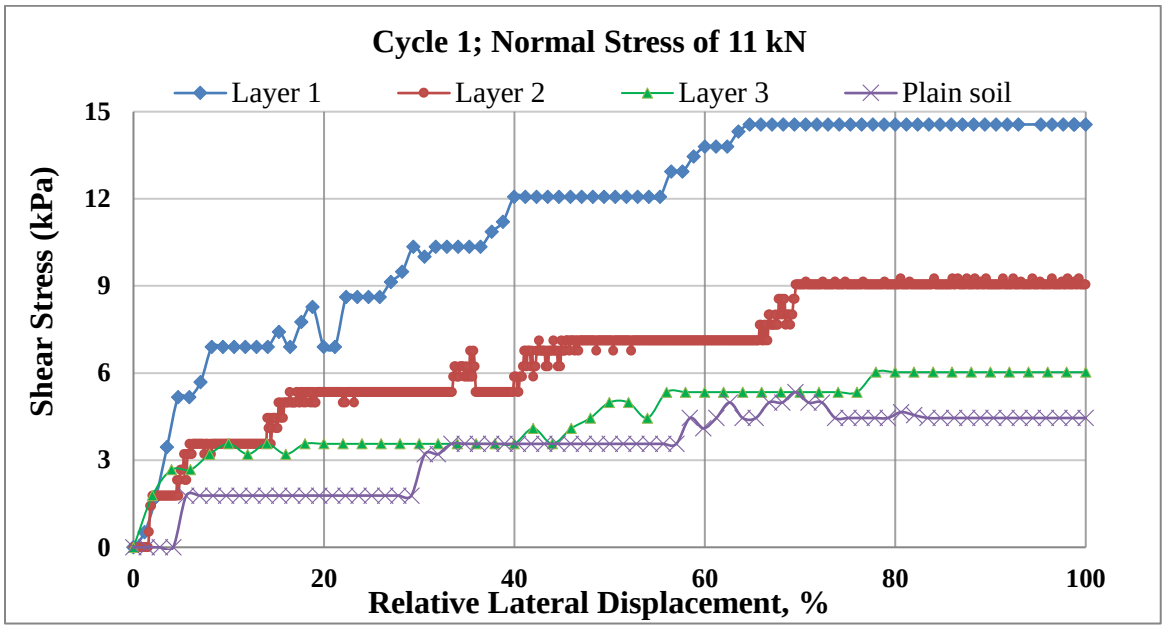

Figure 4.8: Stress-Strain curve for soil samples from Cycle 1 for a normal stress of 11 kN.

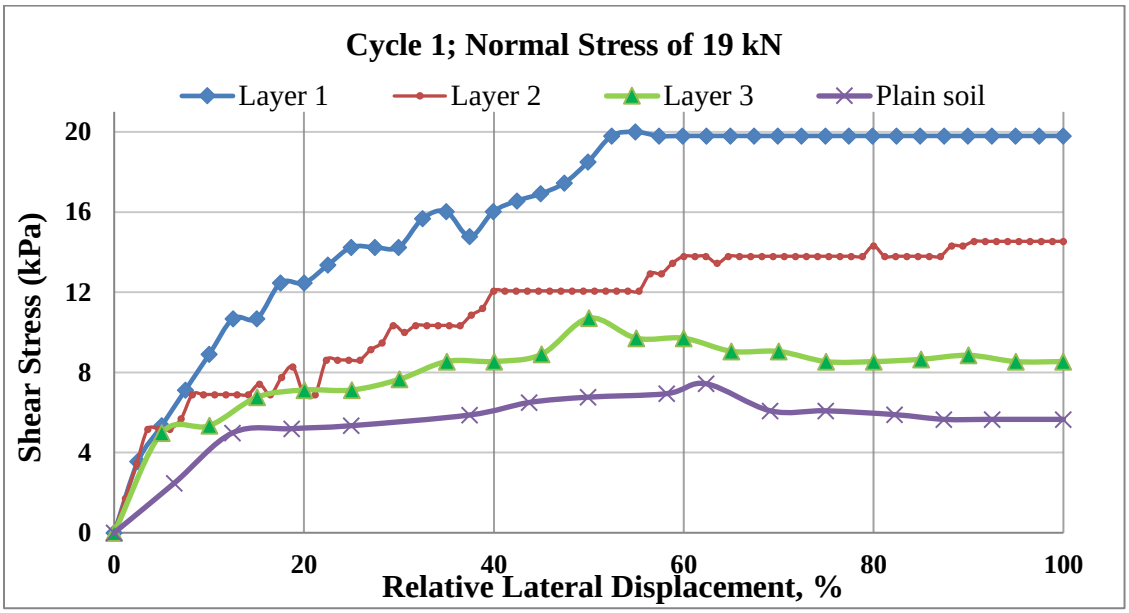

Figure 4.9: Stress-Strain curve for soil samples from Cycle 1 for a normal stress of 19 kN.

For Cycle 3, the highest value of cohesion was found equal to 4.94 kPa for Layer 1 and the minimum value of 2.14 kPa was found for “Plain Soil Layer” as shown in **Table 4.3**. One thing to note over here is that the cohesion value of "Plain Soil" was comparable with that of Cycle 1. Peak shear strength was again obtained higher for all the rooted soil samples. The failure envelope area decreased from Layer 1 to “Plain Soil Layer” gradually. The cohesion of soil increased by approximately 127% for Layer 1, 124% for Layer 2 and almost no increase in cohesion for Layer 3. The result indicates there is a high influence of root reinforcement till the depth of 16 cm after which there is negligible increase in root cohesion. This is different from the result obtained from Cycle 1 where the influence in cohesion was found till the Layer 3. This indicates that roots reinforcement goes deeper in Cycle 1 than in Cycle 3.

Table 4.3: Calculation of values of cohesion (c) and friction angle (ϕ) for Cycle 3.

Normal Stress (kPa)	**Peak Shear Strength (kPa) for Cycle 3**			
	Layer 1 (0-8cm)	Layer 2 (8-16 cm)	Layer 3 (17-24 cm)	Plain Soil (no roots)
5	9.04	6.35	3.55	3.20
11	12	10.85	7.01	5.43
19	19	12.7	9	6.90
Cohesion (c) (kPa)	4.94	4.81	2.07	2.14
Friction Angle (ϕ)	35.76°	23.83°	20.89°	14.56°

Figure 4.10 shows the Mohr’s failure envelope of soil at different depths in Cycle 3 of the CS-28 project. **Figures 4.11, 4.12 and 4.13** shows the stress-strain curve of the

soil layers in Cycle 3 for different normal load value of 5 kPa, 11 kPa, and 19 kPa respectively.

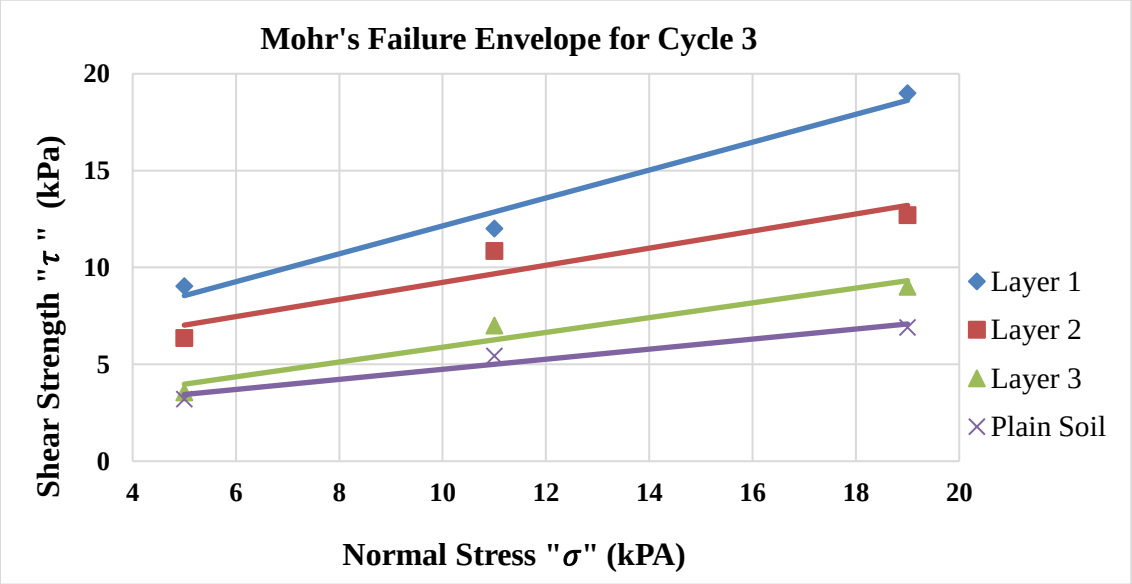

Figure 4.10: Graph of normal stress vs. shear strength for soil samples from Cycle 3 of CS-28.

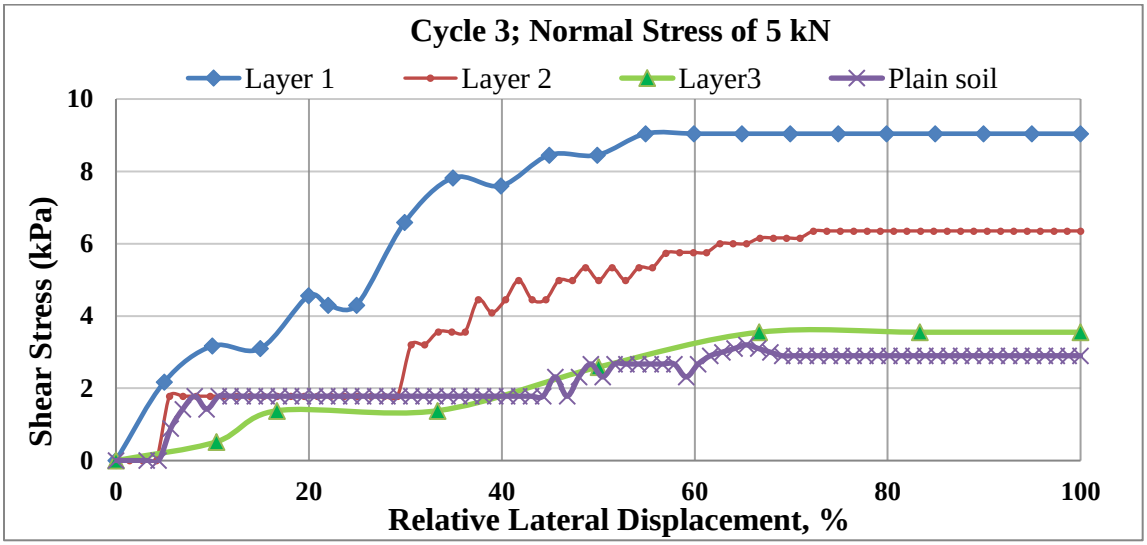

Figure 4.11: Stress-Strain curve, soil samples from Cycle 3 for the normal stress of 5 kN.

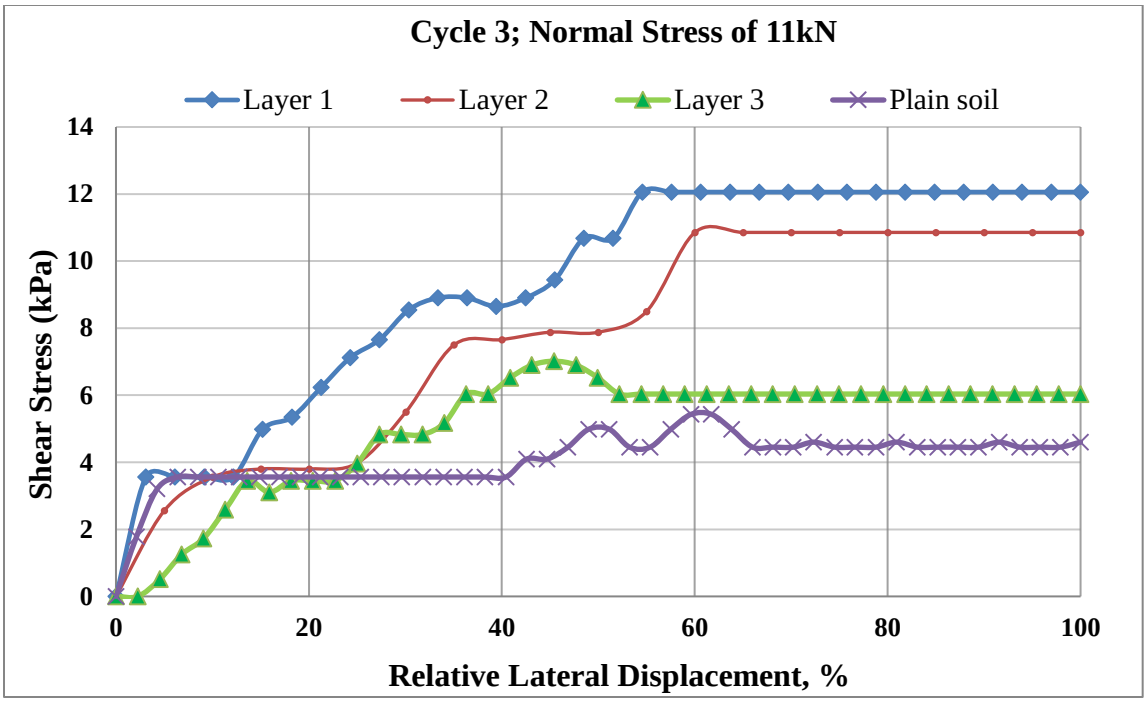

Figure 4.12: Stress-Strain curve for soil samples from Cycle 3 for the normal stress of 11 kN.

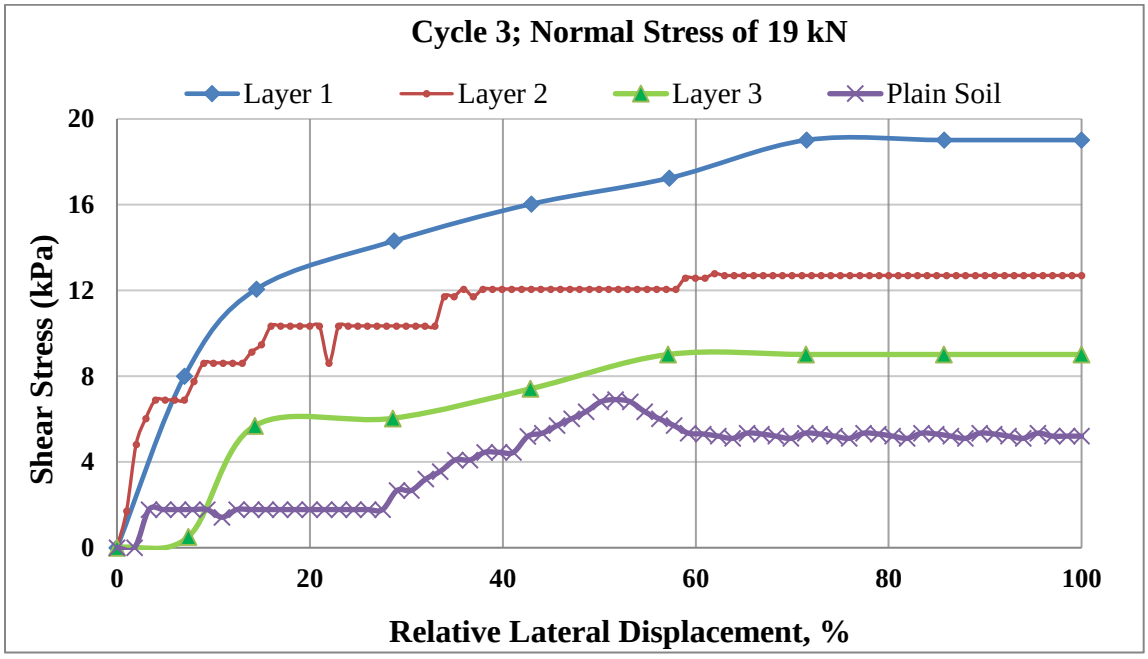

Figure 4.13: Stress-Strain curve for soil samples from Cycle 3 for the normal stress of 19 kN.

4.4 Calculation of c_R and Comparison with Wu *et al.* Model and FBM Model

Root area ratio (*RAR*) values for *Spartina alterniflora* decreased with depth in all sampling locations as seen in previous studies by the authors (Greenway 1987; Schmid & Kazda 2001). Similarly, both the mean root diameters and the number of roots were found to be decreasing with increasing depth for all the sampling locations. For Cycle 1, RAR value of *Spartina alterniflora* ranged between 0.01443 at Layer 1 (0-8 cm) to 0.00363 at Layer 3 (16-24 cm). Cycle 3 had relatively lower *RAR* value which ranged between 0.01085 (1.08 %) at Layer 1 (0-8 cm) to 0.00203 (0.2%) at Layer 3 (16-24 cm) as shown in **Table 4.4**. Root-induced cohesion (c_R) for each layer was calculated by subtracting the total shear strength of that respective layer with the shear strength of "Plain-Soil Layer" obtained from the direct shear test. Root cohesion was also calculated for each layer by first using the Wu *et al*. (1979) model given from **Eq. 2-4** and from the FBM model by using the flowchart presented by Pollen and Simon (2005). Root-induced cohesion (c_R) was found to be decreasing from Layer 1 to Layer 3 of all the soil layers. For Cycle 1, root reinforcement from Wu *et al*. model (c_{WU}) ranged between 54.03 kPa to 17.95 kPa and the root reinforcement from the FBM model (c_{FBM}) ranged between 49.65 kPa to 13.58 kPa. Likewise, for Cycle 3, root reinforcement from Wu *et al*. model (c_{WU}) ranged between 44.96 kPa to 13.05 kPa and the root reinforcement from the FBM model (c_{FBM}) ranged from 27.16 kPa to 10.87 kPa. When these root reinforcement values were compared with those obtained from direct shear tests, it was found that even though FBM model results were relatively more accurate over the Wu *et al*. model, both the model still highly overestimated the root reinforcement. The ratio of root reinforcement

calculated from FBM model to Wu *et al*. model varied between 0.92 to 0.55 which is also shown in **Table 4.4**.

Table 4.4: Comparison of root cohesion from the direct shear test with root cohesion from Wu *et al*. (1979) perpendicular model and FBM model.

Layer	Soil Shear Plane Area (mm2)	Root Type	Average Root Dia. (mm)	No. of Roots	Total Root Area (mm2)	RAR for each Root Type	Average Tensile Strength (kPa)	Root Cohesion c_R (kPa) (Wu *et al*. model)	Root Cohesion c_R (kPa) (FBM model)	Root Cohesion c_R (kPa) (Direct Shear Test)	C_{FBM}/C_{WU}
CYCLE 1											
Layer 1	3166.92	R1	4.57	2	32.83	0.0104	2244.30	54.03	49.65	3.10	0.92
0-8 cm	3166.92	R2	2.54	2	10.13	0.0032	2553.00				
	3166.92	R3	0.76	6	2.74	0.0009	15720.00				
Layer 2	3166.92	R1	4.57	1	16.42	0.0052	2244.30	34.63	19.02	1.70	0.52
8-16cm	3166.92	R2	2.54	2	10.13	0.0032	2553.00				
	3166.92	R3	0.76	4	1.82	0.0006	15720.00				
Layer 3	3166.92	R1	4.57	0	0	0	2244.30	17.96	13.58	0.3	0.76
16-24 cm	3166.92	R2	2.54	2	10.13	0.0032	2553.00				
	3166.92	R3	0.76	3	1.36	0.0004	15720.00				
CYCLE 3											
Layer 1	3166.92	R1	4.57	1	16.42	0.0052	2244.30	44.96	27.16	2.76	0.61
0-8 cm	3166.92	R2	2.54	3	15.20	0.0048	2553.00				
	3166.92	R3	0.76	6	2.74	0.0009	15720.00				
Layer 2	3166.92	R1	4.57	0	0	0	2244.30	31.00	24.45	2.66	0.79
8-16 cm	3166.92	R2	2.54	3	15.20	0.0048	2553.00				
	3166.92	R3	0.76	6	2.74	0.0009	15720.00				
Layer 3	3166.92	R1	4.57	0	0	0	2244.30	13.05	10.87	0	0.83
16-24 cm	3166.92	R2	2.54	1	5.08	0.0016	2553.00				
	3166.92	R3	0.76	3	1.37	0.0004	15720.00				

Several factors contribute to the inaccuracy of these models. Both models put root tensile strength and its diameter as contributing factors to soil reinforcement. However, they do not account for the slipping effects where roots tensile strength is not fully mobilized. Likewise, it is hard to account for the orientation of roots with failure plane and the distortion angle of sheared roots which are vital parameters in these analytical models. Smaller roots increase the uncertainty to measure the diameter of the roots, thereby increasing errors in the estimation of root area ratio (RAR). Moreover, this inaccuracy highly adds up while measuring the tensile strength of these small roots from the measured peak load values. Also, these models only consider the roots tensile strength treating the roots as a stretched cable without considering the bending and compression strength of the roots (Mao *et al.* 2014).

The ratio of actual root cohesion obtained from direct shear test and root cohesion obtained from Wu *et al.* model (without accounting for the orientation factor of roots i.e. 1.2, which is shown in **Eq. 2-4**) was calculated for each of the rooted soil layer. The averaged value of ratio for all the layers of each sampling stations was calculated which was equal to 0.065. This value can be used to modify the root reinforcement coefficient proposed by Wu *et al.* model for *Spartina alterniflora* in dredged soils as shown by **Eq. 4-1**. However, the results from these analytical models, should either be used after proper analysis or should be used only for preliminary estimation:

$$c_R = 0.065 \sum_{i=1}^{n} T_{ri}\left(\frac{A_{ri}}{A}\right) \qquad \textbf{Eq. 4-1}$$

4.5 Delft3D Analysis

Shear stress developed on the soil during Hurricane Ike was calculated from the parameters obtained from Delft3D results. Based on the table of values given by Annadale as discussed in Chapter 2, the calculated value for mass strength number (M_S), block size number (K_B), discontinuity bond strength number (K_D), relative ground structure number or orientation number (J_S) was equal to 0.02, 1, 0.25 and 1 respectively. Erodibility index (K) can be calculated using **Eq. 2-11** as shown in **Eq. 4-2**:

$$K = 0.02 * 1 * 0.25 * 1 = 0.05 \qquad \textbf{Eq. 4-2}$$

For $K \leq 0.1$, critical stream power (P_c) can be calculated using **Eq. 2-9** as shown in **Eq. 4-3**:

$$P_c = 0.48 * K^{0.44} = 0.48 * 0.005^{0.04} = 0.388 \frac{\text{kW}}{\text{m}^2} \qquad \textbf{Eq. 4-3}$$

This value of stream power was assumed to be constant for all over the grid. Two methods as discussed in Chapter 3 were used to calculate the ratio of shear strength to shear stress.

For the first method, maximum bed shear stress and velocity of water for the specific location was obtained using QUICKPLOT. Results were extracted for peak surge condition as discussed in Chapter 3. Analysis was done for all the four grid conditions: Dry grid without vegetation, dry grid with vegetation, submerged grid without vegetation, and submerged grid with vegetation. Maximum bed shear stress obtained from Delft3D was compared with the shear strength of the soil obtained from the laboratory tests. This ratio of shear strength to shear stress was used as a representative factor to define the stability of soil at a location. The soil is safe from erosion if the value is greater than 1;

the higher the value, the more stable the soil will be. **Table 4.5** and bar graph in **Figure 4.14** shows the calculation and illustration of the ratio of shear stress strength to shear stress for each of the sampling stations, respectively.

Table 4.5: Calculation of shear strength to shear stress ratio for six sampling locations for four different grid conditions.

Location (Cycle / Sampling station)	Minimum Soil Shear Strength (kPa)	Dry grid without vegetation			Dry grid with vegetation		
		Maximum Bed Shear Stress (Pa)	Velocity (m/s)	Ratio of Shear strength to Shear stress	Maximum Bed Shear Stress (Pa)	Velocity (m/s)	Ratio of Shear strength to Shear stress
Cycle 1, st. 1	5.4	25	0.45	216	20	0.4	270
Cycle 1, st. 2	5.4	20	0.4	270	15	0.3	360
Cycle 1, st. 3	5	15	0.3	333	12.5	0.2	400
Cycle 3, st. 1	3.6	11	0.35	327	7	0.4	514
Cycle 3, st. 2	4.1	7	0.35	586	5	0.3	820
Cycle 3, st. 3	3.6	12	0.3	300	4	0.35	900
		Submerged grid without vegetation			Submerged grid with vegetation		
Cycle 1, st. 1	5.4	4.5	0.6	1200	1.5	0.25	3600
Cycle 1, st. 2	5.4	5	0.5	1080	1.5	0.2	3600
Cycle 1, st. 3	5	4	0.55	1250	1	0.2	5000
Cycle 3, st. 1	3.6	2	0.4	1800	3	0.35	1200
Cycle 3, st. 2	4.1	3.5	0.35	1171	1.5	0.35	2733
Cycle 3, st. 3	3.6	3.5	0.3	1029	3.5	0.3	1029

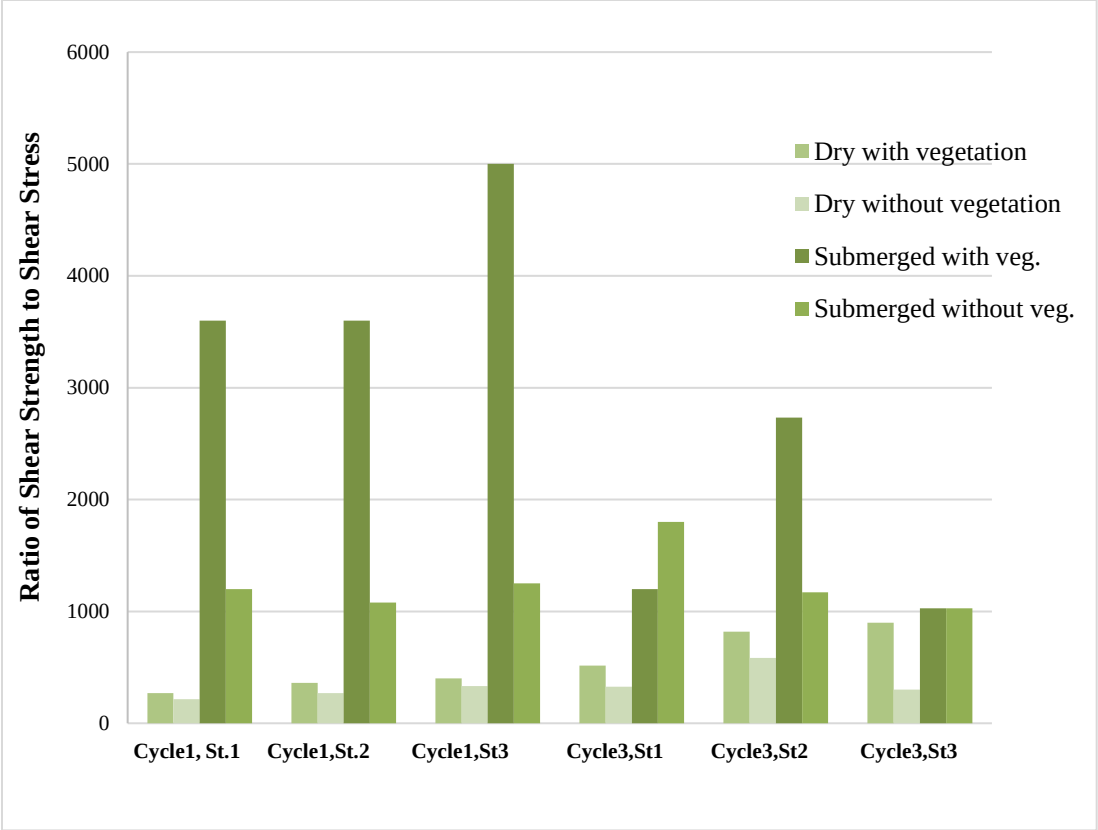

Figure 4.14: Ratio of shear strength to shear stress for six sampling locations for four different grid conditions using Delft3D analysis.

The calculated values of shear strength to shear stress ratio for all the sampling locations was found greater than 1. It shows that all sampling stations were safe from mass erosion during storm conditions of Hurricane Ike.

For the second method, Annadale's Method was used to obtain the ratio of shear strength to shear stress for four different scenarios. The value of critical stream power was calculated from **Eq. 4-2** which is equal to 388 W/m^2. This was assumed constant all over the grid. The analysis was again done for all the four grid conditions. **Table 4.6** and **Figure 4.15** shows the calculation and illustration of the ratio of shear stress strength to shear stress for each of the sampling stations respectively.

Table 4.6: Calculation of shear strength to shear stress ratio for six sampling locations for four different grid conditions using Annadale's Method.

Location (Cycle / Sampling station)	Critical Stream Power (P_c) (W/m^2)	Dry grid without vegetation				Dry grid with vegetation			
		Max. Bed Shear Stress (Pa)	Velocity (m/s)	Power of Waves (P_w)	Ratio of P_c to P_w	Max. Bed Shear Stress (Pa)	Velocity (m/s)	Power of Waves (P_w)	Ratio of P_c to P_w
Cycle 1, st. 1	388	25	0.45	11.25	34	20	0.4	8	49
Cycle 1, st. 2	388	20	0.4	8	49	15	0.3	4.5	86
Cycle 1, st. 3	388	15	0.3	4.5	86	12.5	0.2	2.5	155
Cycle 3, st. 1	388	11	0.35	3.85	101	7	0.4	2.8	139
Cycle 3, st. 2	388	7	0.35	2.45	158	5	0.3	1.5	259
Cycle 3, st. 3	388	12	0.3	3.6	108	4	0.35	1.4	277
		Submerged grid without vegetation				Submerged grid with vegetation			
Cycle 1, st. 1	388	4.5	0.6	2.7	144	1.5	0.25	0.37	1035
Cycle 1, st. 2	388	5	0.5	2.5	155	1.5	0.2	0.3	1293
Cycle 1, st. 3	388	4	0.55	2.2	176	1	0.2	0.2	1940
Cycle 3, st. 1	388	2	0.4	0.8	485	3	0.35	1.05	370
Cycle 3, st. 2	388	3.5	0.35	1.23	317	1.5	0.35	0.52	739
Cycle 3, st. 3	388	3.5	0.3	1.05	370	3.5	0.3	1.05	370

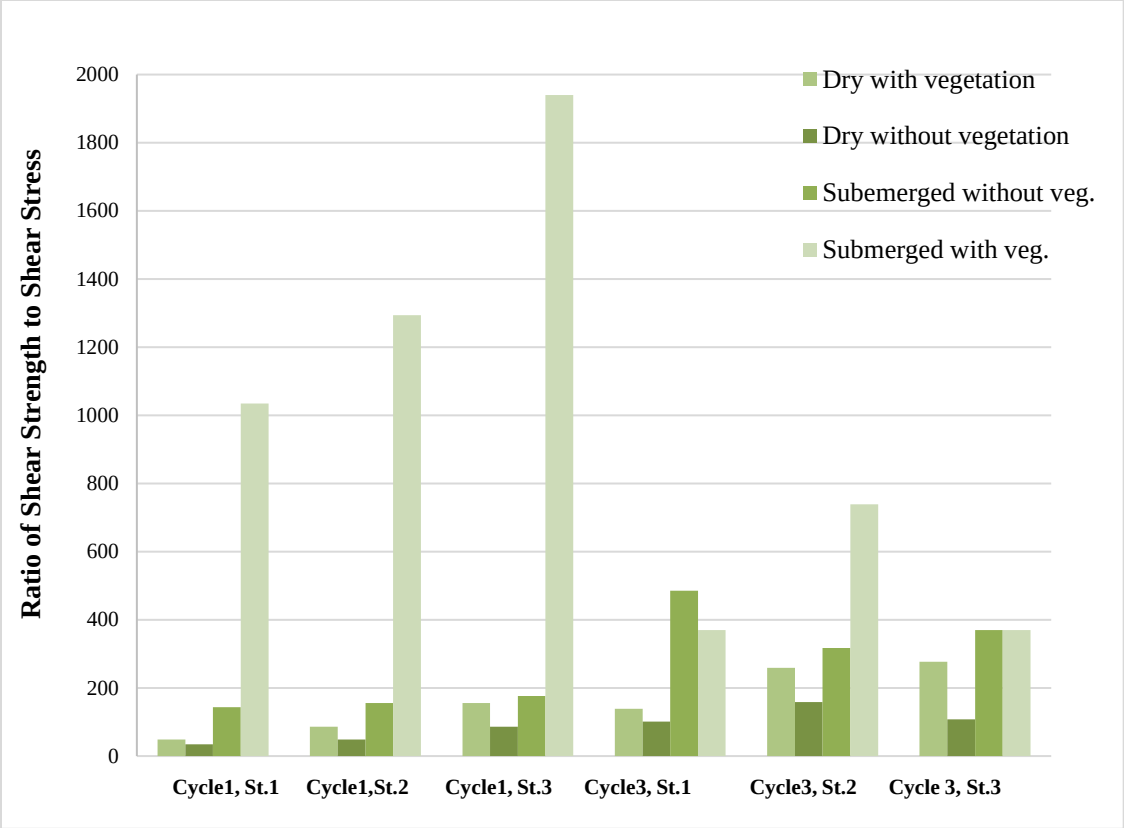

Figure 4.15: Graph showing the ratio of shear strength to shear stress for six sampling locations for four different grid conditions by using Annadale's Method.

Figure 4.15 shows that for all the sampling stations, the ratio of shear strength to shear stress is much higher in the case of submerged grid with the presence of vegetation. The ratio of shear strength to shear stress is the lowest in the case of dry grid without vegetation. The calculated values of shear strength to shear stress ratio for all the sampling locations was far greater than 1 which shows that all sampling stations were safe from mass erosion during storm conditions of Hurricane Ike. If we analyze the overall scenario as "with vegetation" and "without vegetation", we can see that the ratio of shear strength to shear stress for a location is always higher in the presence of vegetation. This indicates that the shoots of the vegetation significantly help to increase the resistance of soil against erosion by reducing the maximum bed shear stress.

CHAPTER 5

CONCLUSION AND FUTURE WORKS

Soil reinforcement study by vegetation is a complex system involving the interaction of several factors. Results from all the tests and analyses on rooted soil illustrate the importance of *Spartina alterniflora* roots in enhancing the shear strength of dredged soil.

Direct shear test on rooted soil and plain soil samples show the decreasing root reinforcement with depth for all the sampling stations. For Cycle 1, reinforcement provided by roots of *Spartina alterniflora* increased the cohesion of the soil by approximately 130% for Layer 1 (0-8 cm), 70% for Layer 2 (8-16 cm) and only 12.5 % for Layer 3 (17-24 cm). Likewise, for Cycle 3, root reinforcement increased the cohesion of soil by approximately 127% for Layer 1, 124% for Layer 2 and almost no increase in cohesion for Layer 3.

Vane shear test results show the corrected value of undrained shear strength and root area ratio, decreases with increasing depth for all the sampling locations. This indicates the direct significance of roots on the un-drained shear strength of soil. The tensile test results show a higher peak load value of large diameter roots. However, when this load value was proportioned with the root diameter, smaller diameter roots had relatively higher tensile strengths.

Wu *et al.* model and the FBM model were used to estimate the root reinforcement value analytically. The results from these models show that even though the FBM model was relatively more accurate over the Wu *et al*. model, both the model still highly overestimated the root reinforcement. Both model put root tensile strength and its diameter as contributing factors to the soil reinforcement. However, they do not account for the slipping effects where root's tensile strength is not fully mobilized. Likewise, it is hard to account for the orientation of roots with failure plane and the distortion angle of sheared roots which are vital parameters in such analytical models. These models only consider the root's tensile strength treating the roots as a stretched cable. They do not account for the bending and compression strength of the roots (Mao *et al*. 2014). Therefore, the results from these analytical models should either be used after proper analysis or for preliminary estimation.

Results obtained from Delft3D Wave FLOW coupled model encompassing the hydrodynamics of Lake Calcasieu estuarine system, with Hurricane Ike forcing was analyzed (Shahriar 2017). Four different scenarios were considered and the time-period during peak surge was chosen for the study. Two different methods were used to calculate the ratio of shear strength to shear stress. For both the methods, the ratio of shear strength to shear stress was found to be relatively higher in the presence of vegetation. This trend can suggest that the shoot of the vegetation can help to increase the erosion resistance potential of the soil by absorbing some of the wave energy.

All the results from the *in-situ* test (vane shear test), lab test (direct shear test), analytical model and numerical analysis using Delft3D demonstrate that the roots of *Spartina alterniflora* provide significant reinforcement to the coastal soils. These results

indicate that *Spartina alterniflora* can be used as a vital reinforcing asset in the newly created dredged lands of coastal Louisiana.

This research experience also suggests that root reinforcement from grass species can be more reliably measured if *in-situ* direct shear test machine or large-scale direct shear machine, which can measure shear strength of large size samples, can be used. The Pull-out tests of the roots can give more accurate value of the soil reinforcement provided by the roots. Sampling of soil and root specimens should be done at different seasons of a year to get a more realistic value of reinforcement provided by the vegetation.

Further research can also be done to correlate the root reinforcement with root density, salinity, pH of soil, aboveground biomass, and distance from the marsh's edge. The critical shear stress of the soil at the marsh bed can be calculated *in-situ* if a cohesive strength meter can be used. Using the jet-erosion test and/or hole erosion test on the rooted soil samples to calculate the erodibility of the rooted soil is the other recommended options.

As for the numerical analysis, the study can be done with a high-resolution grid and a more accurate vegetation model in Delft3D to calculate the wave induced bed shear stress at different locations. Sensitivity analysis of the wave-induced bed shear stress with the variation in distributions of vegetation cover, density and stem diameter in the marshes can be done. Likewise, finite element analysis tools like ANSYS, PLAXIS or ABACUS can be used to study the vegetation reinforcement effect by analyzing the elasto-plastic response of the soil subjected to wave induced bed shear stress.

APPENDIX

ACRONYMS, ABBREVIATIONS, AND SYMBOLS

ASTM	American Society for Testing Materials
c	Cohesion
cm	Centimeter(s)
CPRA	Coastal Protection and Restoration Authority
FBM	Fiber Bundle Model
FEM	Finite Element Method
ft.	foot (feet)
FS	Factor of Safety
in.	inch(es)
kN	kilo Newton(s)
kPa	kilo pascal
lb.	pound(s)
m	meter(s)
mm	millimeter(s)
MPa	Mega Pascal
PI	Plasticity Index
PVC	Poly Vinyl Chloride
RAR	Root Area Ratio
S_u	Undrained Shear Strength
T_r	Tensile strength of root
u	Pore water pressure
φ	Angle of internal friction of soil
μ	Coefficient of friction
2D	Two-dimensional
3D	Three-dimensional

BIBLIOGRAPHY

Anderson, C. E. (1974). "Review of structure in several North Carolina salt marsh plants." *Ecology of Halophytes*, 307-344.

Annandale, G. W. (2006). *Scour technology*. McGraw-Hill.

ASTM D2573. "Standard Test Method for Field Vane Shear Test in Saturated Fine-Grained Soils, ASTM International." *ASTM International, West Consohocken, PA*.

ASTM D3080. "Standard Test Method for Direct Shear Test of Soils Under Consolidated Drained Conditions." *ASTM International, West Consohocken, PA*.

Barras, J. A. (2009). *Land area change, and overview of major hurricane impacts in coastal Louisiana, 2004-08*. US Department of the Interior, US Geological Survey.

Barras, J., Beville, S., Britsch, D., Hartley, S., Hawes, S., Johnston, J., Kemp, P., Kinler, Q., Martucci, A., and Porthouse, J. (2003). *Historical and projected coastal Louisiana land changes: 1978-2050*. United States Geological Survey.

Barry, J. M. (1997). *Rising tide: the great Mississippi flood of 1927 and how it changed America*. Simon and Schuster, New York.

Blum, M. D., Tomkin, J. H., Purcell, A., and Lancaster, R. R. (2008). "Ups and downs of the Mississippi Delta." *Geology*, 36(9), 675–678.

Boesch, D. F., Josselyn, M. N., Mehta, A. J., Morris, J. T., Nuttle, W. K., Simenstad, C. A., and Swift, D. J. (1994). "Scientific assessment of coastal wetland loss, restoration and management in Louisiana." *Journal of Coastal Research*, i–103.

Braja, M. Das. (2008). "Advanced soil mechanics." *Routledge Publication. ISBN*, 415420261(9780415420266), 567.

Broome, S. W., Seneca, E. D., and Woodhouse, W. W. (1988). "Tidal salt marsh restoration." *Aquatic Botany*, 32(1–2), 1–22.

Christiansen, T., Wiberg, P. L., and Milligan, T. G. (2000). "Flow and sediment transport on a tidal salt marsh surface." *Estuarine, Coastal and Shelf Science*, 50(3), 315–331.

Coppin, N. J., and Richards, I. G. (1990). *Use of vegetation in civil engineering*. Construction Industry Research and Information Association London.

Costanza, R., Pérez-Maqueo, O., Martinez, M. L., Sutton, P., Anderson, S. J., and Mulder, K. (2008). “The value of coastal wetlands for hurricane protection.” *AMBIO: A Journal of the Human Environment*, 37(4), 241–248.

Couvillion, B. R., Barras, J. A., Steyer, G. D., Sleavin, W., Fischer, M., Beck, H., Trahan, N., Griffin, B., and Heckman, D. (2011). *Land area change in coastal Louisiana (1932 to 2010)*. US Department of the Interior, US Geological Survey.

CPRA. (2017). *Louisiana’s comprehensive master plan for a sustainable coast*. Coastal Protection and Restoration Authority, Baton Rouge, LA.

Craft, C., Megonigal, P., Broome, S., Stevenson, J., Freese, R., Cornell, J., Zheng, L., and Sacco, J. (2003). “The pace of ecosystem development of constructed Spartina alterniflora marshes.” *Ecological Applications*, 13(5), 1417–1432.

Craft, C., Reader, J., Sacco, J. N., and Broome, S. W. (1999). “Twenty-five years of ecosystem development of constructed Spartina alterniflora (Loisel) marshes.” *Ecological Applications*, 9(4), 1405–1419.

Crone, T. J., and Tolstoy, M. (2010). “Magnitude of the 2010 Gulf of Mexico oil leak.” *Science*, 330(6004), 634–634.

Day, J. W., Boesch, D. F., Clairain, E. J., Kemp, G. P., Laska, S. B., Mitsch, W. J., Orth, K., Mashriqui, H., Reed, D. J., and Shabman, L. (2007). “Restoration of the Mississippi Delta: Lessons from hurricanes Katrina and Rita.” *Science*, 315(5819), 1679–1684.

Day, J. W., Britsch, L. D., Hawes, S. R., Shaffer, G. P., Reed, D. J., and Cahoon, D. (2000). “Pattern and process of land loss in the Mississippi Delta: A spatial and temporal analysis of wetland habitat change.” *Estuaries and Coasts*, 23(4), 425–438.

Deltares. (2011). *User Manual Delft3D-FLOW:* S*imulation of multi-dimensional hydro-dynamic and transportation phenomena, including sediments*. Deltares, Delft, Netherlands.

Dixon, T. H., Amelung, F., Ferretti, A., Novali, F., Rocca, F., Dokka, R., Sella, G., Kim, S.-W., Wdowinski, S., and Whitman, D. (2006). “Space geodesy: Subsidence and flooding in New Orleans.” *Nature*, 441(7093), 587–588.

Dokka, R. K. (2006). “Modern-day tectonic subsidence in coastal Louisiana.” *Geology*, 34(4), 281–284.

Gabet, E. J. (1998). “Lateral migration and bank erosion in a saltmarsh tidal channel in San Francisco Bay, California.” *Estuaries and Coasts*, 21(4), 745–753.

Gedan, K. B., Kirwan, M. L., Wolanski, E., Barbier, E. B., and Silliman, B. R. (2011). "The present and future role of coastal wetland vegetation in protecting shorelines: Answering recent challenges to the paradigm." *Climatic Change*, 106(1), 7–29.

Gray, D. H., and Leiser, A. T. (1982). *Biotechnical slope protection and erosion control.* Van Nostrand Reinhold Company Inc.

Gray, D. H., and Sotir, R. B. (1996). *Biotechnical and soil bioengineering slope stabilization: A practical guide for erosion control*. John Wiley & Sons.

Greenway, D. R. (1987). Vegetation and slope stability. *Slope stability*, 187-230.

Houck, O. A. (1983). "Land loss in coastal Louisiana: Causes, consequences, and remedies." *Tul. L. Rev.*, 58, 3.

Howes, N. C., FitzGerald, D. M., Hughes, Z. J., Georgiou, I. Y., Kulp, M. A., Miner, M. D., Smith, J. M., and Barras, J. A. (2010). "Hurricane-induced failure of low salinity wetlands." *Proceedings of the National Academy of Sciences*, 107(32), 14014–14019.

Le Hir, P., Roberts, W., Cazaillet, O., Christie, M., Bassoullet, P., and Bacher, C. (2000). "Characterization of intertidal flat hydrodynamics." *Continental Shelf Research*, 20(12), 1433–1459.

Mao, Z., Yang, M., Bourrier, F., and Fourcaud, T. (2014). "Evaluation of root reinforcement models using numerical modelling approaches." *Plant and Soil*, 381(1–2), 249–270.

Mazda, Y., Wolanski, E., and Ridd, P. (2007). *The role of physical processes in mangrove environments: Manual for the preservation and utilization of mangrove ecosystems*. Terrapub.

McNutt, M. K., Camilli, R., Crone, T. J., Guthrie, G. D., Hsieh, P. A., Ryerson, T. B., Savas, O., and Shaffer, F. (2012). "Review of flow rate estimates of the Deepwater Horizon oil spill." *Proceedings of the National Academy of Sciences*, 109(50), 20260–20267.

Mehta, A. J. (1991). "Review notes on cohesive sediment erosion." *Coastal Sediments*, ASCE, 40–53.

Micheli, E. R., and Kirchner, J. W. (2002). "Effects of wet meadow riparian vegetation on streambank erosion: Measurements of vegetated bank strength and consequences for failure mechanics." *Earth Surface Processes and Landforms*, 27(7), 687–697.

Millar, R. G., and Quick, M. C. (1998). "Stable width and depth of gravel-bed rivers with cohesive banks." *Journal of Hydraulic Engineering*, 124(10), 1005–1013.

Miller, M. (2014). "*Operations, maintenance and monitoring report for Sabine Refuge Marsh Creation Project (CS-28), Coastal Protection and Restoration Authority of Louisiana* ". Coastal Protection and Restoration, Lafayette, Louisiana.

Mitsch, W. J., Day Jr, J. W., Gilliam, J. W., Groffman, P. M., Hey, D. L., Randall, G. W., and Wang, N. (2001). "Reducing Nitrogen Loading to the Gulf of Mexico from the Mississippi River Basin: Strategies to Counter a Persistent Ecological Problem. *BioScience*, 51(5), 373–388.

Mitsch, W. J., and Jørgensen, S. E. (2004). *Ecological engineering and ecosystem restoration*. John Wiley & Sons.

Moeller, I., Spencert, T., and French, J. R. (1996). "Wind wave attenuation over saltmarsh surfaces: Preliminary results from Norfolk, England." *Journal of Coastal Research*, 1009–1016.

Morton, R. A., Buster, N. A., and Krohn, M. D. (2002). "Subsurface controls on historical subsidence rates and associated wetland loss in southcentral Louisiana." *Gulf Coast Association of Geological Societies Transactions*, v. 52, 767-778.

Owens, E. H., Santner, R., Cocklan-Vendl, M., Michel, J., Reimer, P. D., and Stong, B. (2011). "Shoreline treatment during the Deepwater Horizon-Macondo response." *International Oil Spill Conference Proceedings (IOSC)*, American Petroleum Institute.

Pollen, N., and Simon, A. (2005). "Estimating the mechanical effects of riparian vegetation on stream bank stability using a fiber bundle model." *Water Resources Research*, 41(7).

Redfield, A. C. (1972). "Development of a New England salt marsh." *Ecological Monographs*, 42(2), 201–237.

Reed, D. J., and Wilson, L. (2004). "Coast 2050: A new approach to restoration of Louisiana coastal wetlands." *Physical Geography*, 25(1), 4–21.

Schmid, I., and Kazda, M. (2001). "Vertical distribution and radial growth of coarse roots in pure and mixed stands of Fagus sylvatica and Picea abies." *Canadian Journal of Forest Research*, 31(3), 539–548.

Shahriar, M. M., Wang, J. X., Alam, S., and Patterson, W. B. (2016). "Soil-binding ability of vegetation roots in enhancing erosion resistance of a shallow slope." *International Journal of Geotechnical Engineering*, 10(4), 409–417.

Shahriar, M. M. (2017). "Numerical and Experimental Studies on Coastal Marsh Erosion under Hurricane induced Wave and Current", PhD thesis, Department of Civil Engineering, Louisiana Tech University.

Shinkle, K. D., and Dokka, R. K. (2004). *Rates of vertical displacement at benchmarks in the lower Mississippi valley and the northern Gulf Coast*. US Department of Commerce, National Oceanic and Atmospheric Administration, National Ocean Service, National Geodetic Survey.

Streever, W. J. (2000). "*Spartina alterniflora* marshes on dredged material: A critical review of the ongoing debate over success." *Wetlands Ecology and Management*, 8(5), 295–316.

Thomas, R. E., and Pollen-Bankhead, N. (2010). "Modeling root-reinforcement with a fiber-bundle model and Monte Carlo simulation." *Ecological Engineering*, 36(1), 47–61.

Turner, R. E. (2011). "Beneath the salt marsh canopy: Loss of soil strength with increasing nutrient loads." *Estuaries and Coasts*, 34(5), 1084–1093.

Turner, R. E., McKee, K. L., Sikora, W. B., Sikora, J. P., Mendelssohn, I. A., Swenson, E., Neill, C., Leibowitz, S. G., and Pedrazini, F. (1984). "The impact and mitigation of man-made canals in coastal Louisiana." *Water Science and Technology*, 16(3–4), 497–504.

Waldron, L. J. (1977). "The shear resistance of root-permeated homogeneous and stratified soil." *Soil Science Society of America Journal*, 41(5), 843–849.

Wayne, C. J. (1976). "The effects of sea and marsh grass on wave energy." *Coastal Research Notes*, 4(7), 6–8.

Winterwerp, J. C., and Van Kesteren, W. G. (2004). *Introduction to the physics of cohesive sediment dynamics in the marine environment*. Elsevier, New York.

Wu, T. H., McKinnell III, W. P., and Swanston, D. N. (1979). "Strength of tree roots and landslides on Prince of Wales Island, Alaska." *Canadian Geotechnical Journal*, 16(1), 19–33.

Zedler, J. B. (2000). "Progress in wetland restoration ecology." *Trends in Ecology & Evolution*, 15(10), 402–407.

Zreik, D. A., Krishnappan, B. G., Germaine, J. T., Madsen, O. S., and Ladd, C. C. (1998). "Erosional and mechanical strengths of deposited cohesive sediments." *Journal of Hydraulic Engineering*, 124(11), 1076–1085.